Applied Catalysis B: Environmental 252 (2019) 138–151

Contents lists available at ScienceDirect

Applied Catalysis B: Environmental

journal homepage: www.elsevier.com/locate/apcatb

Experimental and computational study of Tm-doped TiO_2: The effect of Li^+ on Vis-response photocatalysis and luminescence

Paweł Mazierski[a,b], Pablo Nicolás Arellano Caicedo[a], Tomasz Grzyb[c], Alicja Mikolajczyk[a], Juganta K. Roy[d], Ewelina Wyrzykowska[e], Zhishun Wei[b,f], Ewa Kowalska[b], Tomasz Puzyn[e], Adriana Zaleska-Medynska[a], Joanna Nadolna[a,b,*]

[a] Department of Environmental Technology, University of Gdansk, 80-308, Gdansk, Poland
[b] Institute for Catalysis, Hokkaido University, Sapporo, 001-0021, Japan
[c] Department of Rare Earths, Faculty of Chemistry, Adam Mickiewicz University in Poznan, 60-780, Poznan, Poland
[d] Interdisciplinary Center for Nanotoxicity, Department of Chemistry, Physics and Atmospheric Sciences, Jackson State University, Jackson, MS, 39217, USA
[e] Laboratory of Environmental Chemometrics, University of Gdansk, 80-308 Gdansk, Poland
[f] Hubei Provincial Key Laboratory of Green Materials for Light Industry, Hubei University of Technology, Wuhan, 430068, China

ARTICLE INFO

Keywords:
TiO_2
Thulium
Lithium
Visible light
PDOS

ABSTRACT

The utilization of solar light to induce a photocatalytic reaction in the presence of wide band gap semiconductors requires the modification of their surface and optical properties. The Vis-to-UV up-conversion process (UCP) that occurs in lanthanide ions could be employed to induce TiO_2. Thus, having in mind solar-forced photocatalysis, nanostructured TiO_2 co-modified with Tm and Li was prepared via a hydrothermal method. In addition to the exhaustive surface characterization of the as-prepared samples, the partial density of states (PDOS) was computed to better understand the electronic structure and physicochemical properties of the prepared photocatalysts. It was demonstrated that Tm ions were beneficial for phenol degradation in the aqueous phase under visible irradiation, whereas the co-presence of Tm and Li ions was profitable for enhanced luminescence. Although action spectra revealed that excitation of Tm-TiO_2 in the range from 400 to 490 nm led to the photodegradation of phenol and 2-propanol, the UCP was not responsible for the photocatalytic activity under Vis irradiation. Therefore, it is proposed that the formation of sub-band gap states from the lanthanide *4f* level played a key role in the phenol degradation process.

1. Introduction

Titanium dioxide has shown great potential for use as almost ideal and powerful photocatalyst for various significant reactions due to its multifunctionality. Even though TiO_2 is active only under UV irradiation and has low quantum efficiency, it is still considered an ideal candidate to be developed as a visible light active photocatalyst due to its physical and chemical stability, strong oxidation capacity and low cost of production [1–4]. In recent years, much attention has been drawn to the preparation of TiO_2 modified with rare earth (RE) metals exhibiting activity under visible light irradiation. According to the recent literature, lanthanide ions can improve substrates' adsorption onto the TiO_2 surface, shift the absorption edge of TiO_2 into the visible region and increase the temperature of anatase to the rutile transformation [5]. One of the available visible light activation mechanisms for RE-TiO_2 photocatalysts is the up-conversion process (UCP), which is realized through the chains of ground and excited state absorption [6]. As indicated in our previous review paper [5], only four lanthanide ions can theoretically be employed to sensitize TiO_2 through the Vis-to-UV up-conversion process: Er^{3+}, Ho^{3+}, Nd^{3+} and Tm^{3+}. However, there are only a few studies regarding Tm-modified TiO_2 photocatalysts. For example, a low-temperature hydrolysis reaction [7,8] and a ball-milling method [9] were used to obtain Tm-doped TiO_2 samples, with the photocatalytic activity evaluated via the methylene blue degradation process under UV light irradiation using an actinic lamp (λ = 360 nm). It was found that the photocatalytic activity of the Tm-TiO_2 samples was approximately 50% higher than that of the pristine TiO_2 [7]. However, the photocatalytic activity under Vis irradiation and the influence of the UCP on the photocatalytic activity were not investigated. Recently, Parnicka et al. [10] examined the influence of the UCP on the photocatalytic activity of Nd-TiO_2 powders. It was observed that the UCP was not responsible for the photocatalytic activity under visible

* Corresponding author at: Department of Environmental Technology, University of Gdansk, 80-308, Gdansk, Poland.
E-mail address: joanna.nadola@ug.edu.pl (J. Nadolna).

https://doi.org/10.1016/j.apcatb.2019.03.051
Received 12 November 2018; Received in revised form 12 March 2019; Accepted 17 March 2019
Available online 01 April 2019
0926-3373/

light irradiation due to the low intensity of the RE emission [5]. Therefore, it was proposed that co-doping could be a solution to overcome the low emission efficiency of the RE ions [11]. Indeed, the incorporation of Li^+ into RE-doped materials distorted the close environment of the RE ion [12] and/or broke the RE ion pairing, modifying the local crystal field that influenced the RE emission and providing charge compensation [13]. For example, Milicevic et al. [14] observed that the Li^+ co-doping of Eu-TiO_2 lengthened the lifetime of the Eu^{3+} $^5D_0$ excited state and improved the Eu^{3+} emission intensity by up to 37.5%.

Here, for the first time, it has been investigated how Li co-modification affects the structural, optical and photocatalytic properties of Tm-modified TiO_2. To draw the conclusion and provide a possible excitation mechanism under visible light, action spectra measurements were investigated for the photodegradation of phenol and 2-propanol. Diffuse reflectance spectroscopy, X-ray diffraction, BET surface area measurements, X-ray photoelectron spectroscopy and photoluminescence analyses were performed. To understand the electronic structure and physicochemical properties of the prepared photocatalysts, the partial density of states (PDOS) for the developed *molecular* models was calculated.

2. Experimental section

2.1. Preparation of Tm- and Tm-Li-modified TiO_2

The photocatalysts for this study were prepared by a simple hydrothermal method. The procedure used was as follows: 16 ml of titanium isopropoxide (TTIP, 97%) and 136 ml of isopropanol were mixed in a beaker with continuous stirring for 30 min. Then, another solution composed of 4.8 ml of H_2O, 4.8 ml of isopropanol, 1.6 ml of HNO_3 (65%), and the required amounts of thulium nitrate and lithium nitrate (for the Li-Tm-TiO_2 samples) was prepared under continuous stirring for 30 min. The second solution was incorporated slowly into the first solution and mixed for 1 h, and the resulting solution was transferred to a Teflon-lined autoclave. The hydrothermal reaction was carried out at 120 °C for 4 h. The solution was washed many times with water and separated by centrifugation (6000 rpm), and the obtained white powder was dried overnight at 80 °C. Finally, the samples were calcined at 450 °C for 2 h (2 °C/min). Samples with different amounts of thulium (0.1, 0.25, 0.5 and 1.0 mol.%) and lithium (0.5, 1.0, 2.0 and 5.0 mol.%) incorporated into the TiO_2 were prepared. Reference samples, namely, pristine TiO_2 and 2.0Li-TiO_2 (2.0 mol% Li), were also synthesized according to the above procedure.

2.2. Characterization of Tm- and Tm-Li-modified TiO_2

The following apparatuses were applied to characterize the obtained samples: (1) the photoabsorption properties were recorded using a Shimadzu UV–Vis spectrophotometer, (2) nitrogen adsorption-desorption isotherms were obtained using a Micromeritics Gemini V, (3) XRD patterns were recorded using a Rigaku diffractometer (RINT Ultima+), (4) the oxidation states of the elements and the surface compositions of the samples were determined by X-ray photoelectron spectroscopy (XPS) with a JEOL JPC-9010MC (MgKa X-ray) spectrometer, (5) the emission spectra were measured by a Princeton Instrument PIXIS:256E Digital CCD Camera equipped with an SP-2156 Imaging Spectrograph and Opolette 355LD UVDM tuneable laser as the excitation source (repetition rate of 20 Hz; pulse energy of 0.5 mJ at 250 nm and 4 mJ at 476 nm), an FEL0500 optical filter and ADBU-20 Pellin Broca prism were used during the measurements, (6) morphology was investigated by scanning transmission electron microscopy (STEM) using Hitachi HD-2000, Tokyo, Japan.

2.3. Photocatalytic tests

2.3.1. Phenol degradation under visible light (polychromatic irradiation)

Photocatalytic degradation tests were carried out using a 1000 W lamp with a 420 nm cut-off filter, with constant aeration (5 dm^3/h) and a cooling system used for the reactor and the lamp (10 °C), which also served for the absorption of the infrared irradiation. 25 ml of phenol (0.21 mM) and 125 mg of photocatalyst were added into the photoreactor and mixed using an ultrasonic bath for 10 min and a magnetic stirrer for 30 min. Then, the visible irradiation was started. Every 10 min, a 0–5 ml sample was taken from the reactor and filtered using a syringe filter (pore size of 0.1 μm). The phenol concentration and formed intermediates were determined by a high-performance liquid chromatography (HPLC, Shimadzu) system equipped with a Kinetex C18 column (150 mm x 3 mm; particle size of 2.6 μm; pore diameter of 100 Å). The flow rate was maintained at 0.4 ml/min with a mobile phase composed of acetonitrile and water (v/v: 7.5/92.5), with the SPD-M20 A diode array detector operated at 205, 225 and 254 nm.

2.3.2. Hydroxide radical (˙OH) determination (polychromatic visible irradiation)

The determination of the hydroxide radical formation was carried out using a terephthalic acid (TPA) solution ($5{\cdot}10^{-4}$ M in $2{\cdot}10^{-3}$ M NaOH), which forms a highly fluorescent product, 2-hydroxyterephthalic acid, after reaction with hydroxyl radicals. The procedure was almost the same as that used during the phenol degradation test, except for the amount of the sample used for the luminescence analysis (1.7 ml) and sampling time (0, 20, 40 and 60 min). The fluorescence intensity was measured by a luminescence spectrophotometer (Perkin Elmer LS 50B).

2.3.3. Photocatalytic degradation in the presence of scavengers (polychromatic visible irradiation)

To investigate the impact of the reactive oxygen species on the photocatalytic activity of the most active sample, phenol degradation in the presence of various scavengers, such as silver nitrate, ammonium oxalate, benzoquinone and tert-butanol, was carried out. The phenol aqueous solution containing the abovementioned scavengers (C_0 = 0.21 M, 1:1) and photocatalyst was subjected to the same experimental procedure as that described in Section 2.3.1.

2.3.4. Action spectra analysis (monochromatic irradiation)

Action spectra analysis was performed for the most active sample and pristine TiO_2 as a reference for decomposition of phenol and 2-propanol under monochromatic irradiation using a diffraction grating-type illuminator (Jasco, RM-FD) equipped with a 300-W xenon lamp (Hamamatsu, C2578-02). A suspension composed of photocatalyst (50 mg) and phenol (5 ml C_0 = 0.21 M) or 2-propanol (5 ml, 5 vol.%) was introduced into a quartz cell and irradiated at monochromatic wavelengths for 90 min (λ = 400, 420, 440, 460, 467, 470, 480, 490, 500, 520, 540 and 560 nm), 180 min (λ = 625, 685, 675 and 730 nm) and 360 min (λ = 795 nm). The irradiation intensity was adjusted by a steel mesh and measured for each wavelength by an optical power metre (HIOKI 3664). During the photocatalytic degradation, the suspension was continuously stirred. The samples for the HPLC/GC-FID analysis were collected in 30-min time intervals and filtrated via syringeless filters (Whatman Mini-UniPrep, PVDF). The HPLC analysis was performed for phenol with a WAKOSIL-II SC18 AR column (250 mm 4.6 mm) with parameters as follows: a flow rate of 1 ml/min, a mobile phase of acetonitrile, water and phosphoric acid (60/39/1 v/v/v), a sample injection volume of 5 μL, and the detector operated at 254 nm. The 2-propanol oxidation was investigated by measurement of acetone concentration GC/FID using a Shimadzu GC-14B gas chromatograph equipped with a flame ionization detector (GC/FID).

The apparent quantum efficiency as a function of the wavelength was calculated based on the ratio of the rate of electron consumption

(rate of benzoquinone and acetone generation) to the flux of incident photons, assuming that two photons are required according to the reaction stoichiometry.

2.4. Theoretical study

The theoretical calculations were carried out using the Vienna *ab initio* simulation package (VASP) implementing spin-polarized density-functional theory (DFT) and the generalized gradient approximation (GGA) by Perdew-Burke-Ernzerhof (PBE) with intra-site Coulomb interactions between Ti-3*d* electrons in Dudarev's approach (here called the PBE + *U* method) [15–17]. To avoid failure in describing strongly correlated 3*d* electrons localized on Ti atoms, particularly in the case of reduced anatase (101), we used a *U* value of 3.5 eV, which has been found to be required for a proper description of the anatase crystal compared to experiments [18]. In this study, the ionic cores and valence electrons for Li-1 s^2 and Ti-[Ne]3s^2 (core) and the Tm atom 5 $s^2$5$p^6$6$s^2$4f^{13} (treated as valence electrons) are described by a projector-augmented wave potential (PAW) with a cut-off energy of 400 eV and a Γ-centred Monkhorst-Pack grid with a separation of 0.03 $Å^{-1}$ (equivalent to a *k*-point mesh of 8 × 8x11 for bulk anatase, and 2 × 2x1 for TiO_2 (101)-*c*(4 × 2) supercells), and the total energy was converged to < 1 meV/atom. All the structures considered in this study were fully relaxed until all the forces were < 0.02 eV $Å^{-1}$ and 10^{-6} eV/atom [5,18]. The PBE + *U* computed optimal lattice parameters for bulk anatase TiO_2 were $a = b = 3.85$ Å, $c = 9.72$ Å. The anatase TiO_2(101) surface was modeled in Periodic Boundary Conditions (PBC) with three O-Ti-O layers (Fig. 1) along the [001] direction and 15 Å vacuum thickness between slabs (resulting in 25 Å in the *z*-direction). All the atoms in the system are allowed to relax except the bottom O-Ti-O layer that is kept fixed to mimic the bulk structure. To investigate the RE metals adsorption on anatase TiO_2(101), we employed a *c*(4 × 2) surface supercell with 144 atoms in order to avoid interaction between atoms and defects in neighboring cells. The modified Li-TiO_2(101) and Li-Tm-TiO_2(101) systems were modelled with oxygen and titanium surface (V_O^{sur}/V_{Ti}^{sur}) and subsurface (V_O^{sub}/V_{Ti}^{sub}) vacancies, respectively.

In this work we also study the adsorption energy (ΔE_{ads}) and surface formation energy (E^f_{Surf}) for the lanthanides (RE) supported by the TiO_2(101) surface were computed using Eqs. (1) and (2), respectively [19].

$$\Delta E_{ads} = E_{tot} - (E_{TiO_2} + E_{Re}) \quad (1)$$

where ΔE_{ads} is the adsorption energy of the cluster as a whole, E_{tot} is the total energy of the interacting rare metal (RE) and the TiO_2 system; E_{TiO_2} is the total energy of the most stable TiO_2 slab; E_{Re} is the total energy of the rare metal in its most stable gas-phase configuration.

According to Ullah et al. [20] and Safaei et al. [21] and the surface formation energy (E^f_{Surf}) was calculated using Eq. (2):

$$E^f_{Surf} = \frac{E_0^{Slab} - nE_{TiO_2}^{Bulk}}{2A} \quad (2)$$

where, E_0^{Slab} is the total energy of the perfect surface, $E_{TiO_2}^{Bulk}$ is bulk energy per formula unit in the bulk, *n* is the number of formula unit in supercell, *A* is the surface area of slab and E^f_{Surf} is surface formation energy.

According to Safaei at al. and Ullah et al. the surface formation energy (E^f_{Surf}) was calculated using Eq. (2) [20,21]. The calculated anatase (101) surface (9 atomic layers) formation energy is 0.48 J/m^2 and is in good agreement with Sanches et al. [19]. In our study, Tm doping was performed by the substitution of either oxygen or titanium atom. So we report here substitution energy for each type of doping. Tm substitution energy, E_{Tm}^{sub}, computed by the following relationship:

$$E_{Tm}^{sab} = E_{0sur}^{Slab-Tm} - e_0^{Slab} + NE_{atom}^{bulk} \quad (3)$$

where, $E_{V0sur}^{Slab-Tm}$ is the total energy of the Tm doped slab (with surface or subsurface oxygen vacancy), E_{Atom}^{Bulk} equilibrium energy per atom and *N* is the number of substituted atoms.

3. Results and discussion

3.1. Diffuse reflectance spectroscopy (DRS)

Results from DRS measurements performed on Tm-TiO_2 and Tm-Li-TiO_2 samples in the spectral range of 200–1100 nm are presented in Fig. 1a) and b), respectively. Pristine TiO_2 and Li-TiO_2 were used as the reference samples. Each sample exhibited an absorption band in the UV range due to charge transfer from the O 2p valence band to the Ti 3d conduction band [20–22]. All modified TiO_2 samples showed a slight redshift in their absorption edges compared to that of pristine TiO_2. The redshifts can be attributed to the charge-transfer transition between the Tm *f* electrons and the titanium dioxide conduction/ valence band [23] or the creation of extrinsic defects in the grain boundary [24]. The spectra for Tm-TiO_2 and Tm-Li-TiO_2 showed additional absorptions due to the *f-f* electronic transitions of the Tm ions at approximately 467, 685 and 795 nm (the transition from the $^3H_6$ ground state to the excited states of thulium $^1G_4$, $^3F_{2/3}$ and $^3H_4$) [25]. Obviously, the intensity of the thulium absorption bands increased with the Tm-ion concentration, which is in agreement with the available literature on rare earth metal TiO_2 modification [10].

3.2. X-ray diffraction (XRD) and BET surface area

The XRD patterns for a) TiO_2, Tm-TiO_2 and b) Li-TiO_2, Tm-Li-TiO_2

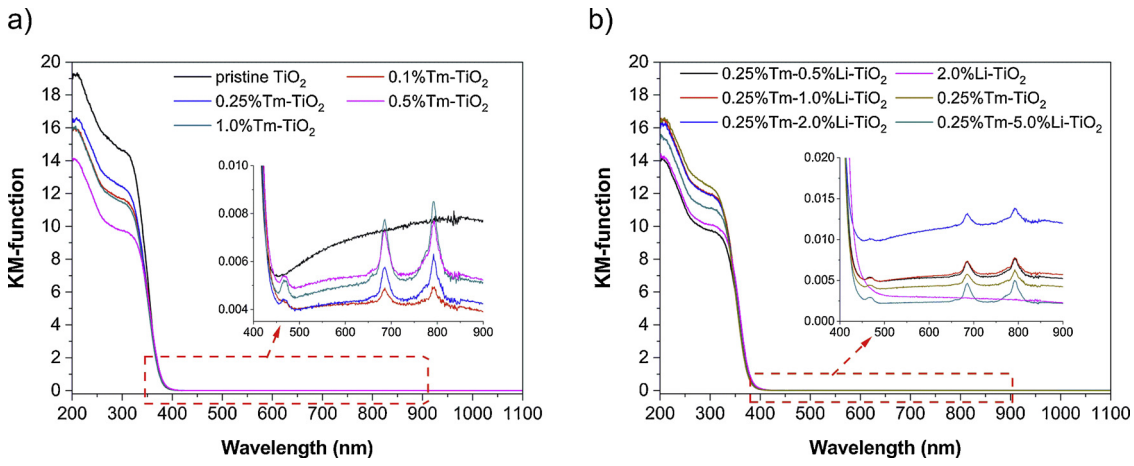

Fig. 1. UV–Vis Kubelka–Munk absorption spectra of a) Tm-TiO_2 and b) Tm-Li-TiO_2 photocatalysts compared to pristine TiO_2 and Li-TiO_2.

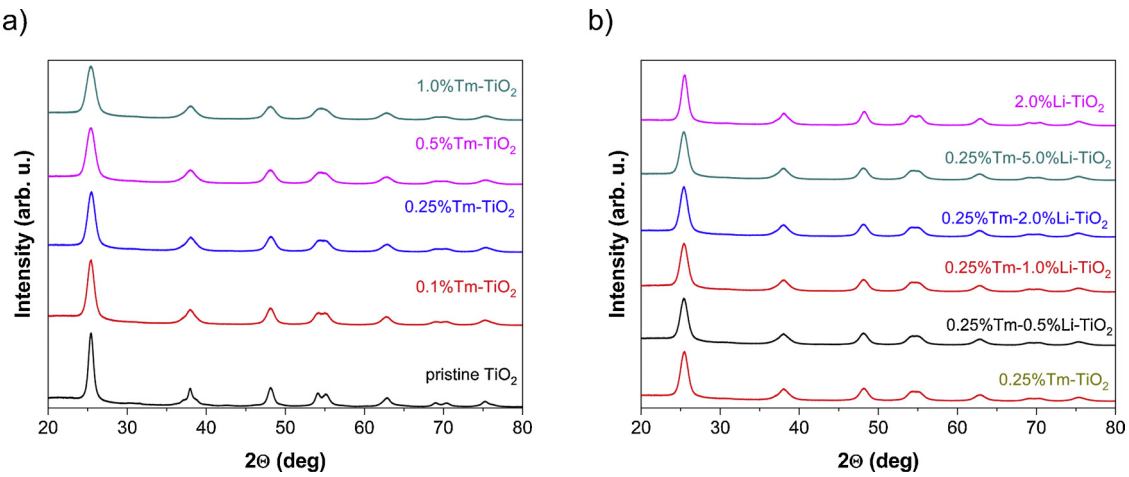

Fig. 2. X-ray diffraction patterns of a) TiO_2, Tm-TiO_2 and b) Li-TiO_2, Tm-Li-TiO_2 photocatalysts.

Table 1
Structural parameters and photocatalytic activity of pristine and modified TiO_2 photocatalysts.

Sample label	BET surface area (m^2/g)	XRD					Phenol degradation (%) under Vis light ($\lambda > 420$ nm)
		Crystallite size (nm)	a = b (A)	c (A)	Crystallite volume (A^3)	Crystalline phase	
Pristine TiO_2	106.8	18.8	3.7825	9.4883	135.75	Anatase	7
0.1%Tm-TiO_2	128	10.9	3.7864	9.4997	136.20	Anatase	19
0.25%Tm-TiO_2	134.4	8.7	3.7025	9.5141	136.84	Anatase	22
0.5%Tm-TiO_2	156.4	6.4	3.7869	9.4995	136.23	Anatase	16
1.0%Tm-TiO_2	155.5	6.2	3.7879	9.4972	136.27	Anatase	12
0.25%Tm-0.5%Li-TiO_2	132.2	7.2	3.7909	9.5056	136.60	Anatase	11
0.25%Tm-1.0%Li-TiO_2	141.5	8.2	3.7906	9.5060	136.59	Anatase	16
0.25%Tm-2.0%Li-TiO_2	139.9	8.4	3.7913	9.5096	136.69	Anatase	18
0.25%Tm-5.0%Li-TiO_2	138.6	8.5	3.7842	9.4816	135.78	Anatase	13
2.0%Li-TiO_2	111.2	7.2	3.7814	9.4856	135.63	Anatase	6

are shown in Fig. 2. The diffraction peaks can be ascribed to the (101), (004), (200) and (105) crystallographic planes of TiO_2 anatase (JCPDS database), where the most intense (101) peak appeared at $2\theta = 25.4^\circ$ [26]. The heat treatment at 450 °C did not cause anatase to undergo a rutile phase transformation. The diffraction peaks for Tm_2O_3 were not observed in any of the Tm-modified photocatalysts, which might suggest that (i) the concentration of Tm ions and/or the Tm_2O_3 crystal sizes were too small for detection, (ii) amorphous, (but not crystalline) oxides were formed, (iii) the Tm oxides were highly dispersed on the titania surface [27,28]. The peaks (101) in the XRD patterns for the Tm-modified TiO_2 samples are slightly wider than the peak for pristine TiO_2, which indicates the effects of the thulium ions on titania NPs formation. It is assumed that surface adsorbed Tm ions inhibited the growth of titania crystallites (as proved by smaller crystallite sizes (Table 1)). Additionally, the possibility of thulium ions impact on the unit cell of TiO_2 could not be neglected, as shown in Table 1 [29].

The BET surface area, crystallite size and cell parameters for the photocatalysts are shown in Table 1. All Tm- and Tm/Li-modified samples showed higher specific surface areas than the pristine TiO_2 photocatalyst (106.82 m^2/g), similar to the data reported for other RE-modified titania samples [8,9,30]. The average crystallite size of the anatase ranged from 6.2 to 10.9 nm for Tm-TiO_2 and 7.2–8.5 for Tm-Li-TiO_2. For pristine TiO_2 and Li-TiO_2 the crystallite size was 18.8 and 7.2 nm, respectively. A decrease in the size of the crystallites was observed with the increasing Tm-ion concentration and after the Li-ion modification of the Tm-TiO_2 photocatalysts. Thulium ions, with a much greater ionic radius (87 pm), could not substitute Ti^{4+}, with a smaller ionic radius (61 pm), in the TiO_2 lattice [4,31]. Such a mismatch of the ionic radii favours the formation of Ti—O—RE bonds (i.e., surface modification) or RE_2O_3 oxides at the surface of the anatase nanoparticles [28]. Therefore, it is proposed that Ti—O—Tm bonds can inhibit the growth of TiO_2 crystal grains, similarly to Nd-modified titania [10]. To determine the possible influence of modification on the unit cell parameters, a Rietveld analysis of the XRD patterns was performed (Table 1). A slight increase in the crystallite volume for the Tm-TiO_2 samples was observed in comparison to pristine TiO_2, which can suggest interstitial doping. The highest crystallite volume was observed for the 0.25%Tm-TiO_2 sample (136.84 A^3). In the case of co-modified samples, the unit cell volume was lower than that of the 0.25% Tm-TiO_2 sample.

3.3. Morphology

The morphology of pristine and modified samples (mono-modified: 0.25%Tm-TiO_2, 2.0%Li-TiO_2 and bi-modified: 0.25%Tm-2.0Li-TiO_2) was investigated by STEM, and obtained data are shown in Fig. 3. Interestingly, it was found that pristine titania was composed of smaller NPs (some of them even of 5-nm size) than modified samples. Although, these data suggest opposite tendency than XRD and BET results (smaller crystallite and larger specific surface area for modified samples), they could be easily explained by co-existence of amorphous titania of fine NPs in pristine sample. Indeed, calculated particle size (from BET, i.e.,

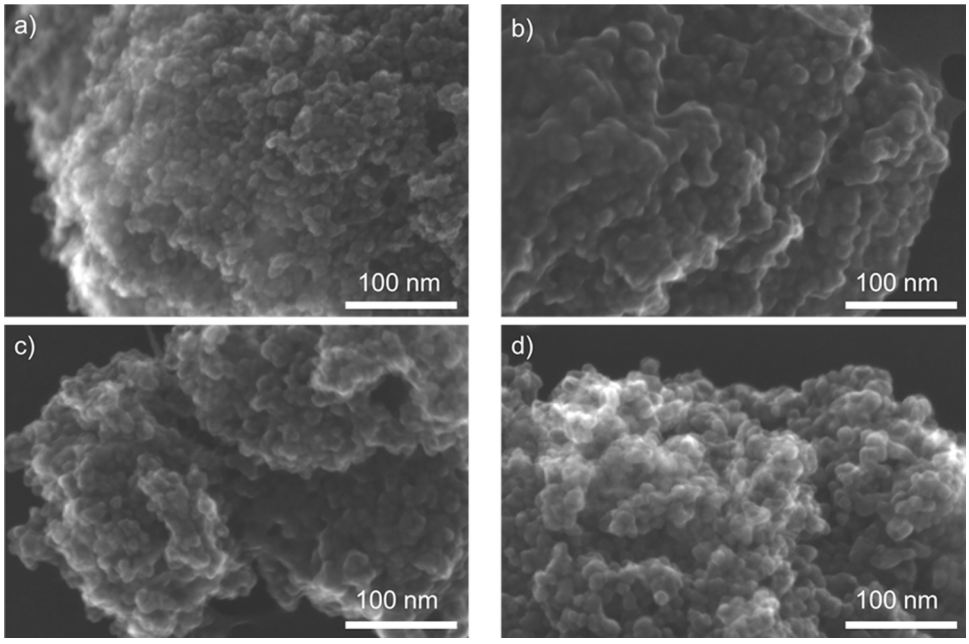

Fig. 3. STEM images of pristine TiO_2 (a), 0.25%Tm-TiO_2 (b), 2.0%Li-TiO_2 (c), 0.25%Tm-2.0Li-TiO_2 (d).

1500/BET) for pristine titania is smaller (14 nm) than crystallite one (18.8), confirming the presence of amorphous titania (undetectable by XRD) of much smaller sizes than anatase crystallites. It should be pointed that in contrast for all modified samples, the calculated particle sizes were larger than crystallite ones, suggesting that modifiers enhanced titania crystallization (less content of fine amorphous titania). Moreover, it was found that morphology of modified samples differed significantly from that by pristine titania, i.e., the particles seemed to be connected by surface modifier (looking like a glue). Therefore, it was confirmed that titania was mainly surface modified by both kinds of modifiers.

3.4. X-ray photoelectron spectroscopy (XPS)

The chemical composition of three modified (0.25%Tm-TiO_2, 0.25%Tm-2.0%Li-TiO_2 and 2.0%Li-TiO_2) and pristine titania samples was analysed by XPS measurements, and the data obtained are shown in Tables 2 and 3. The banding energies for titanium, oxygen and carbon were estimated after deconvolution in accordance with published reports of the XPS analysis of pristine and metal-modified titania samples [6,27]. Exemplary XPS peaks after deconvolution for Ti $2p_{3/2}$, O 1s, and C 1s are shown in Fig. 4. The ratio of oxygen to titanium (Table 2) was approximately stoichiometric (2.0) for the pristine and modified samples, indicating that the metal (Li and Tm) modification did not significantly change the surface structure of the titania, which is reasonable considering the low content of the modifiers. However, a slight decrease in the O/Ti ratio for the samples containing Tm suggests that Tm can replace the hydroxyl groups adsorbed onto the titania surface, which is commonly observed for surface-modified titania samples [32]. Interestingly, the ratio of carbon to titanium (C/Ti) decreased by metal modification, especially for samples containing thulium. It was found that the surface of the modified samples was enriched with Li (24.5% for 2.0%Li-TiO_2 and 28.8% for 0.25%Tm-2.0%Li-TiO_2) and poor in Tm (0.08% for 0.25%Tm-TiO_2 and 0.06% for 0.25%Tm-2.0%Li-TiO_2), suggesting that Li was mainly deposited onto the surface whereas Tm was also found inside the titania lattice (titania doping), as confirmed by the XRD results (Table 1). Interestingly, the low content of Tm and large content of Li in the bimetallic sample (0.25%Tm-2.0%Li-TiO_2) suggests some segregation of metals during

Table 2
Surface compositions of pristine and metal-modified samples determined by XPS analysis.

Sample label	Content (at.%)					Ratio	
	Ti	O	C	Tm	Li	O/Ti	C/Ti
Pristine TiO_2	15.59	34.94	49.47	–	–	2.2	3.2
0.25%Tm-TiO_2	20.66	38.13	41.14	0.08	–	1.9	2.0
0.25%Tm-2.0%Li-TiO_2	16.17	29.52	25.45	0.06	28.8	1.8	1.6
2.0%Li-TiO_2	12.89	28.01	34.65	–	24.45	2.2	2.7

Table 3
Fractions of oxidation states of Ti, O and C from deconvolution of XPS peaks of Ti 2p3/2, O 1 s and C 1 s.

Sample label	Ti $2p_{3/2}$ (%)		O 1 s (%)			C 1 s (%)		
	Ti^{4+}	Ti^{3+}	TiO_2	Ti-OH[a]	Ti-OH[b]	C-C	C-OH	C = O
Pristine TiO_2	98.1	1.9	65.0	23.2	11.8	89.3	2.9	7.8
0.25%Tm-TiO_2	96.1	3.9	75.8	13.8	10.5	37.1	54.9	8.0
0.25%Tm-2.0% Li-TiO_2	95.4	4.6	80.6	11.1	8.3	39.5	52.0	8.5
2.0%Li-TiO_2	95.4	4.6	68.7	17.6	13.7	57.7	31.2	11.1

Ti-OH[a]: Ti-(OH)-Ti/Ti_2O_3/C = O, Ti-OH[b]: Ti-OH/C.-OH.

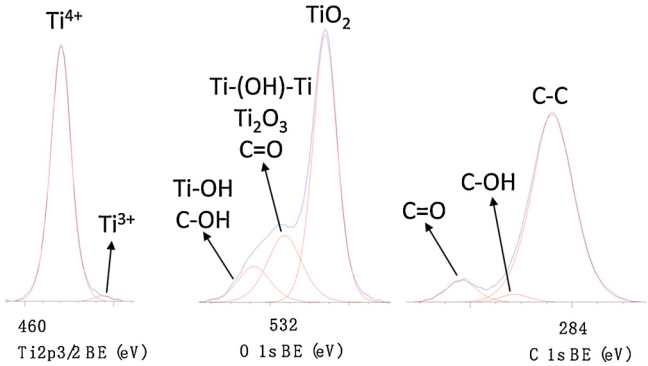

Fig. 4. XPS results for Ti 2p3/2, O 1 s, and C 1 s of pristine TiO_2 sample.

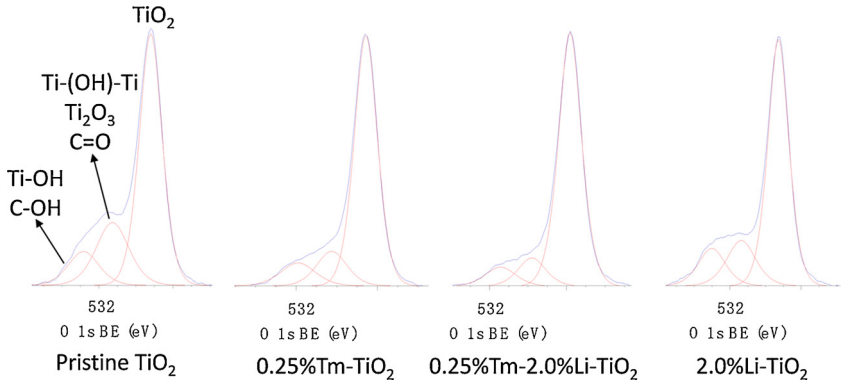

Fig. 5. XPS results for O 1 s for pristine and metal-modified TiO_2 samples.

the deposition, e.g., the direct deposition of Li onto the titania surface and on Tm. The obtained data also suggest that TiO_2 surface was enriched with either very fine Li nanoclusters or atomically dispersed lithium. Considering the mean free path of electrons in TiO_2 to be ca. 2–3 nm, and thus measuring depth for XPS being ca. 6–9 nm (3 × free path of electrons), and crystalline sizes of modified TiO_2 to be 6–11 nm, it could be assumed that not all TiO_2 particles would be measured (especially for larger NPs). Moreover, it should be pointed that XRD analysis gives only average/mean data, and amorphous TiO_2 could not be detected. Summarizing, it is obvious that TiO_2 surface is enriched with lithium. However, it is impossible to evaluate its exact content (only surface one from XPS).

The deconvolution of the oxygen peak (Fig. 5) into three peaks suggests the presence of three forms of oxygen, i.e., (i) lattice oxygen in TiO_2, (ii) C═O, Ti_2O_3 and OH groups bound to two titanium atoms, and (iii) hydroxyl groups bound to titanium and carbon (Ti—OH and C—OH), ca. 529.2 eV, 531.3 eV and 532.9 eV, respectively [33]. It is thought that the metals replaced mainly the hydroxyl groups adsorbed onto the surface of the titania since a significant increase in the content of lattice oxygen (TiO_2) and a decrease in the content of hydroxyl oxygen (—OH) were observed after titania modification, as shown in Table 3. For example, pristine TiO_2 possessed 65.0% of oxygen in the form of TiO_2, whereas modification with Li (2.0%Li-TiO_2) and Tm (0.25%Tm-TiO_2) resulted in increases in the oxygen content to 68.7% and 75.8%, respectively. Considering the O/Ti ratio (Table 2) and the distribution of the oxygen forms (Table 3) in the samples, it is proposed that hydroxyl groups can be adsorbed onto Li likewise onto a titania surface (same O/Ti ratio and a similar content of lattice oxygen as in the pristine samples). Moreover, some synergy was found for the bi-metallic sample (0.25%Tm-2.0%Li-TiO_2), which possessed the highest content of lattice oxygen (80.6%).

Considering the chemical state of the titanium, all of the modified and pristine TiO_2 samples consisted of mainly Ti^{4+}, with the content of the reduced form of titanium (Ti^{3+}) in the range of 1.9%–4.6% (Table 3). Interestingly, metal modification resulted in an increase in the content of Ti^{3+} for all samples, suggesting that the presence of the modifier can disturb the formation of titania crystals (i.e., possible doping), as suggested by the XRD data (Table 1).

Additionality, high carbon content (approximately 34–50 at.%) in the samples is a common phenomenon, which is associated with the method of obtaining a photocatalyst (e.g. use of carbon compounds for synthesis – in our case titanium isopropoxide, isopropanol and ethanol), its storage and performing analysis (adsorption of carbon compounds from the air). The adsorption of carbon compounds on the TiO_2 surface and their impact we have shown in our previous paper [34]. The XPS results presented in this paper suggested adsorption of carbon compounds on the TiO_2 surface instead of carbon doping. The only way to remove carbon from the surface is to repeatedly wash the sample after receiving and storage under inert gas conditions (even calcination at higher temperatures does not remove carbon from TiO_2 [35]). The presence of adsorbed carbon does not change the physicochemical properties of the materials but affects the rate of photocatalytic degradation [34] because the carbon compounds from the TiO_2 surface will always be degraded firstly and then model pollution. Thus, carbon was not included in the physicochemical properties modeling.

3.5. Photoluminescence spectroscopy

The synthesized photocatalysts were analysed by measuring the emission under UV (250 nm) and blue (476 nm) laser excitation. In

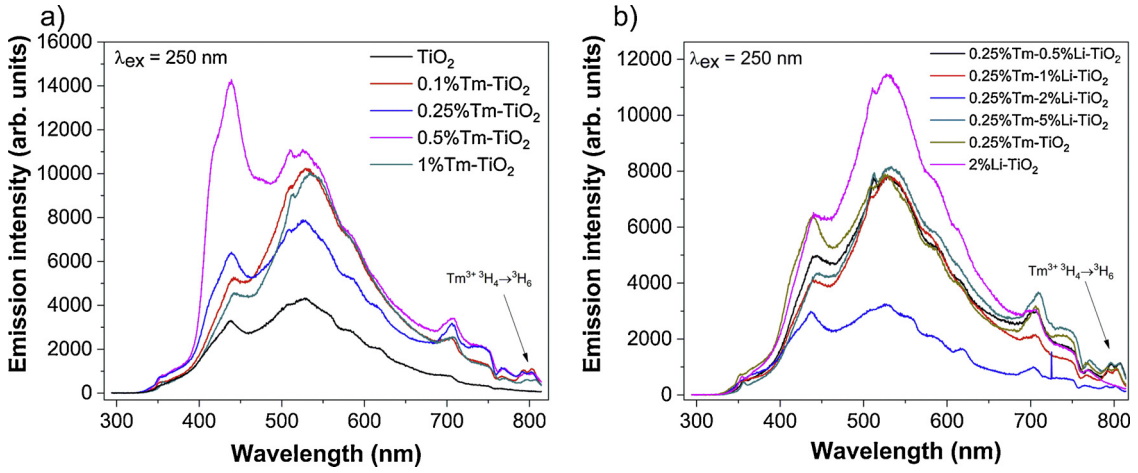

Fig. 6. Emission spectra of TiO_2 photocatalysts under UV laser excitation, doped with (a Tm^{3+} or (b Tm^{3+} and Li^+ ions.

Fig. 6a and b, broad emission bands can be observed, ranging from 350 to 800 nm, with a maximum at approximately 525 nm. This observation shows the typical emission for pristine TiO_2 resulting from the absorption of high-energy photons and the formation of charge carriers and vacancies [4,36]. The complex structure of the TiO_2 emission bands is usually explained by the overlapping of the peaks associated with oxygen vacancies with one (F^- centres) or two (F^+ centres) trapped electrons, with maxima below 525 nm [37]. Other emission peaks might also be deconvoluted from the broad band, with a maximum at approximately 625 nm; they are indicated to be a consequence of the Franck-Condon principle and the polarizability of the lattice ions surrounding the formed vacancies [36]. Additionally, at higher wavelengths (approximately 700 nm), minor peaks connected to the setup used for emission measurements can be observed. As the excitation source, a Nd:YAG pumped tunable laser (OPO) was used. To obtain 250 nm laser wavelength, OPO is pumped by 355 nm laser beam. Despite used optical filters, small remaining of this pumping light may interfere at diffraction grating and generate secondary maxima at $2 \times 355\ nm = 710\ nm$.

The energy absorbed by the TiO_2 host can be transferred to the Tm^{3+} dopant ions, which is observed as minor emission peaks at approximately 800 nm. At this wavelength, emission resulting from the $^3H_4 \rightarrow {}^3H_6$ transition of the Tm^{3+} ions is usually observed [38]. The remaining transitions for the Tm^{3+} ions were not observed due to the overlapping TiO_2 emission. The presence of emission peaks for Tm^{3+} confirmed effective doping into the host structure and the high crystallization of the as-prepared photocatalysts.

The emission of the TiO_2 host compound was enhanced by Tm^{3+} doping, as shown in Fig. 6a. However, as the samples partially decomposed under UV laser radiation, it is impossible to correlate the changes in the spectra with the Tm^{3+} concentration. Single-doping by Li^+ ions also resulted in a higher emission intensity for the TiO_2 host (see Fig. 6b). The dopant ions influenced the effectiveness of the F^+ and F^- formation by the introduction of defects into the crystal structure as well the surface of the TiO_2. Double TiO_2 modification with Li^+ and Tm^{3+} ions also resulted in an enhancement of the emission from TiO_2; however, the effect was lower than in the case of single-modified materials. The introduction of RE^{3+} ions into the TiO_2 structure probably influenced the band gap width of TiO_2, which also affects its emission [39]. The TiO_2 band gap structure is dependent on the structure and morphology of the product as well as the synthesis method, which results in differences in the shape and maximum of the TiO_2 emission peak [27,40,41].

The Tm^{3+} ions embedded in the TiO_2 structure also exhibited luminescence under direct excitation by laser pulses with a wavelength of 476 nm. The absorption of light with this particular wavelength resulted in a transition from the $^4H_6$ ground state into the $^1G_4$ excited state (see also the diffusion reflectance spectra in Fig. 1a and b for the absorption peaks) [42]. As a result of relaxation processes in the Tm^{3+} ions from the $^1G_4$ excited state, emission at longer wavelengths was observed, as shown in Fig. 7. The radiative relaxation to the $^2F_4$ excited state results in emission at approximately 655 nm (the $^1G_4 \rightarrow {}^3F_4$ transition). The non-radiative relaxation from the $^1G_4$ to the $^3F_2$ state, e.g., by cross-relaxation to the neighbouring Tm^{3+} ions, preceded another electronic transition resulting in emission at approximately 675 nm ($^3F_2 \rightarrow {}^3H_6$ transition). Tm^{3+} ions in their $^1G_4$ or $^3F_2$ excited states may also undergo an alternative process (such as multiphoton relaxation), which results in relaxation to the $^3H_4$ excited state. Next, the relaxation to the $^3H_6$ ground level led to emission at approximately 800 nm ($^3H_4 \rightarrow {}^3H_6$ transition) [42].

The characteristics of the emission bands observed in Fig. 7 are typical for 4f-4f transitions of lanthanide ions in their +3 oxidation state – Ln^{3+} (besides La^{3+} and Lu^{3+} ions, which have empty and filled 4f subshells, respectively). The observed peaks are usually narrow with well-defined maxima and low sensitivity for the ion surroundings. This property is a result of the shielding effect of the outer 5s and 5p

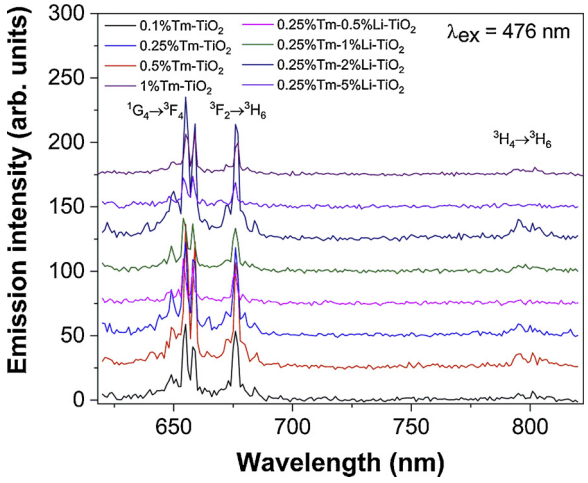

Fig. 7. Emission spectra of TiO_2 photocatalysts modified with Li + and Tm^{3+} ions under 476 nm laser excitation.

electronic shells on the inner 4f subshell [43]. Hence, the shapes and maxima of the observed peaks were similar to those of the spectra measured for all the photocatalysts. The intensities of the emission peaks changed as a result of cross-relaxation in the case of single-doped TiO_2 products, showing that a doping level above 0.5% quenched the emission from the Tm^{3+} ions. This observation is a typical property of Tm^{3+} ions, which are known to be sensitive to concentration quenching [44,45]. Double-modification by Li^+ ions also had an effect on the Tm^{3+} emission intensity. A sample modified with 0.25% of Tm^{3+} and 2% of Li^+ ions showed the most intense emission. Co-modification with Li^+ ions may influence the structure of the host material by creating distortions around the Tm^{3+} and breaking the symmetry of its sites [46]. The modified crystal field around the luminescent Ln^{3+} centres can cause a more effective population of their excited states as well as a reduction in the non-radiative decay [13,47]. However, co-modification by Li^+ ions also has limitations in their concentration, above which a decrease in emission intensity is usually observed [13,46,47]. Higher amounts of Li^+ co-modification may result in the formation of structural defects and quenching centres, which lower the emission from the Ln^{3+} luminescence activators. UCP was not observed under laser excitation at 476, 687 and 795 nm.

3.6. Theoretical study

To investigate the electronic structure and physicochemical properties of Tm-, Li- and Tm-Li modified TiO_2 photocatalysts, the partial density of states (PDOS) for developed molecular models was calculated, as shown in Figs. 8 and 9 (Tables 4 and 5). The adsorption energy (ΔE_{ads}) and surface formation energy (E^f_{Surf}) is listed in Tables 4 and 5, respectively. The PDOS and atomic structure for TiO_2 system with surface defect site (V_{Ti}^{sur1}) is presented in Fig. 8a and d respectively. The most stable configuration for the Tm-TiO_2(101) system is shown in Fig. 8b. The surface defect site (V_O^{sur1}) in the Tm-TiO_2(101) system corresponds to the removal of an oxygen atom (O_{2C}). The Tm-TiO_2(101)-V_O^{sur1} system was found to be a semiconductor with the main contribution of the O-2*p* states in the valence band (VB, below Fermi level) and that of the Ti-3*d* states in the conduction band (above the Fermi level), see Fig. 8b. The presence of V_O^{sur1} and the incorporation of Tm atoms into the anatase TiO_2(101) lattice causes shifts in the valence and conduction band (VB/CB) edges and results in the introduction of impurity Tm-5*d* (mainly Tm-d_z^2 and Tm-d_{yz} states) and Tm-4*f* states into the band gap region of the anatase TiO_2(101) surface (Fig. 8b). The most stable configuration for the Tm-TiO_2(101) and Li-TiO_2(101) system with a titanium surface defect site (V_{Ti}^{sur1}) that corresponds to the removal of a titanium atom (Ti_{5C}) is shown in

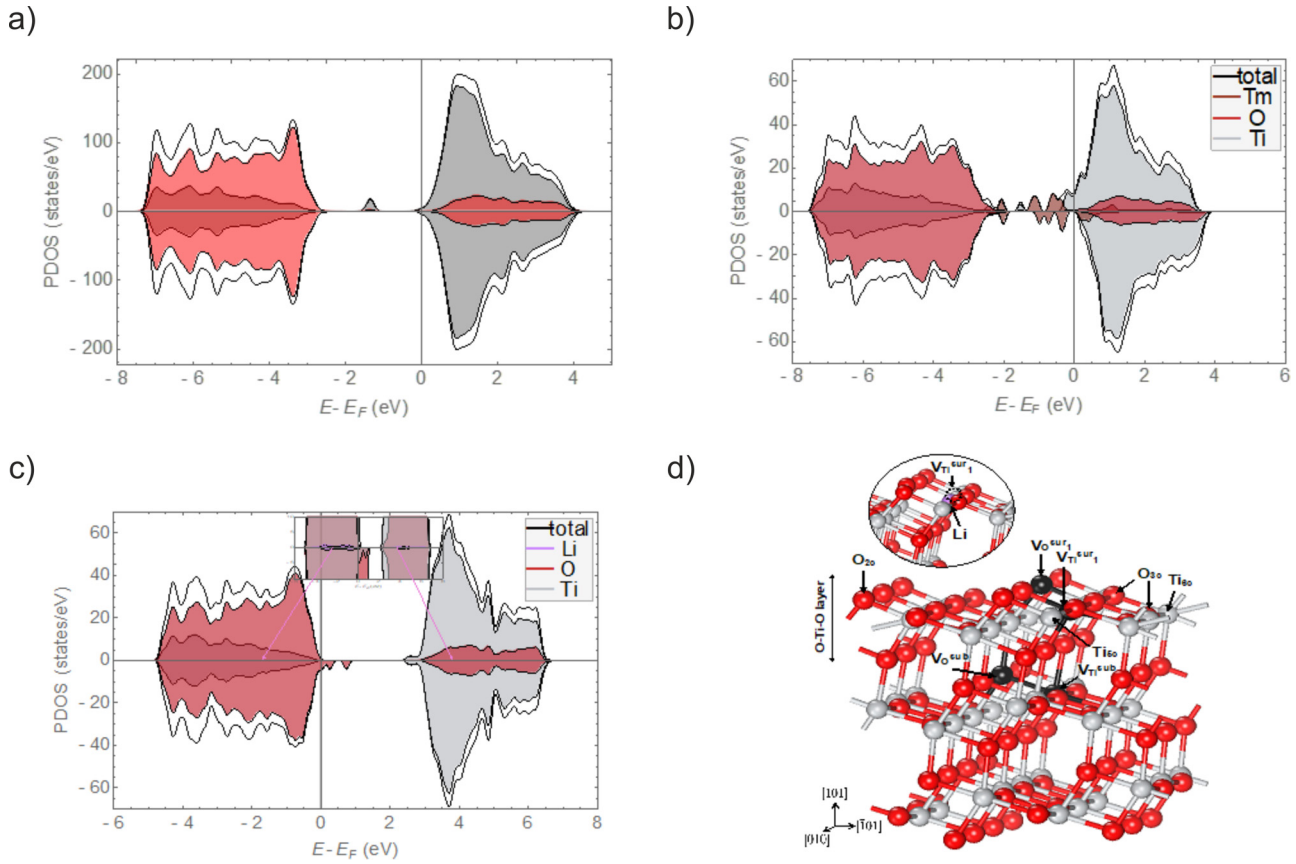

Fig. 8. Spin-polarized PBE + *U* computed PDOS for anatase: (a) TiO_2-V_{O1}^{sur}, (b) Tm-TiO_2-V_O^{sur1}, Li-TiO_2-V_{Ti}^{sur1} system, respectively. (d) Supercell slab model for: RE-TiO_2 system with investigated vacancy sides.

Fig. 8b, c. As shown by the data, the partial density of states (PDOS) for the valence band (VB) of the Li-TiO_2(101)-V_{Ti}^{sur1} system is mainly contributed by the O-2*p* states, with a small contribution from the Ti-3*d* states (Fig. 8c). The valence band (VB, below Fermi level) was dominated by the O-2*p* states. In contrast, the lower conduction band (CB) was dominated by Ti-3*d*, where the peak at 3 eV is due to Ti-$3d_z^2$ (Fig. 8c). The band gap was ~ 2.0 eV (the underestimation of the band gap in comparison to the experimental value is due to the well-known limitations of conventional DFT) [48,49].

The most stable configurations for the Tm-Li-modified TiO_2 photocatalysts with a variety of surface and subsurface titanium/oxygen vacancies are shown in Fig. 9. The surface (V_x^{sur1}) and subsurface defect sites (V_x^{sub1}) in the most stable Tm-Li-TiO_2(101) configurations correspond to the removal of surface/subsurface titanium (Ti_{5C}) and oxygen atoms (O_{2C}), as displayed in Fig. 9b and d, respectively.

The Tm-Li-TiO_2-V_{Ti}^{sur1}-V_{Ti}^{sub1} system is a semiconductor with a band gap value of ~ 2.2 eV. The valence band (VB) of the Tm-Li-TiO_2-V_{Ti}^{sur1}-V_{Ti}^{sub1} configuration had mainly an O-2*p* state character with a small contribution from the Tm-5*d* states (Fig. 9b). The lower conduction band (CB) was dominated by the Ti-3*d* states (mainly Ti-$3d_{x^2-y^2}$ and Ti-$3d_{xz}$). In contrast, the removal of oxygen O_{2C} surface and subsurface atoms from the Tm-Li-TiO_2 configuration (Fig. 9c) as well as the incorporation of Tm^{3+} ions into the anatase TiO_2(101) lattice led to shifts in the valence and conduction band (VB/CB) edges and the introduction of impurity Tm-5*d* and Tm-4*f* states (mainly Tm-d_z^2 and Tm-d_{xy} states) in the band gap region of the anatase TiO_2(101) surface (Fig. 9d).

The results presented here indicate that the incorporation of Tm^{3+} ions into the TiO_2 lattice as well as oxygen vacancies did not only lead to the lattice distortion of the TiO_2 structure (Table 4, Fig. 8a–c) but also affected the electronic structure of the system (Figs. 8b, 9 b, d), such as shifts in the valence and conduction band (VB/CB) edges and the introduction of impurity states (Tm-5*d* states) in the band gap region. It can be expected that induced impurity states that tune the locations of the VB and CB as well as cause the structural distortion of the TiO_2 system may reduce the probability for charge carrier (electron–hole) recombination. Thus, the presence of impurity Tm-5*d* states near the VB and CB may trap photoexcited electrons and holes, thereby inhibiting their recombination and resulting in a higher observed photocatalytic activity for the Tm-TiO_2-based photocatalysts (Table 1). Moreover, the presence of Tm and Li metals in the Tm-Li-TiO_2-V_{Ti}^{sur1}-V_{Ti}^{sub1} system resulted in a higher electronic density in the band gap region, which is related to the Tm-5*d*/4*f* and Ti-3*d* states. Interestingly, in the case of the Tm-TiO_2-V_O^{sur1} system, the densities of the Tm-5*d*/4*f* and Ti-3*d* states in the band gap region were much lower. It can be expected that a higher electron density in the Tm-Li-TiO_2-V_{Ti}^{sur1}-V_{Ti}^{sub1} system may result in enhanced photoluminescence properties. However, the formation of structural defects in the Tm-Li-TiO_2-V_{Ti}^{sur1}-V_{Ti}^{sub1} system may increase charge carrier recombination, resulting in decreased photocatalytic properties. Moreover, narrowing band gap of RE-doped TiO_2 system in comparison with clean anatase TiO_2(101), correlates with the presence of *f*-electron states derived from RE atoms (Fig. 8). Obtained results are in agreement with literature [18,50,51]. For example, Ullah et al. have shown that polypyrrole/$Ti_{16}O_{32}$ composites have narrow band gap and better visible light absorption capability compared to individual constituents [50]. In another study [52,53] authors have found that both the oxygen vacancy and Se-doped $BiVO_4$ semiconductor have ideal band bands and small effective masses of electrons and holes, responsible for high photocatalytic activities. While the Safaei at al. [54] reported that the presence of interplanar hydrogen elements in g-C_3N_4/$BiVO_4$ induced the formation of V^{4+}, elevating its charge carrier mobility. Comparative analyses of both experimental and theoretical studies affirmed that V^{4+} produced

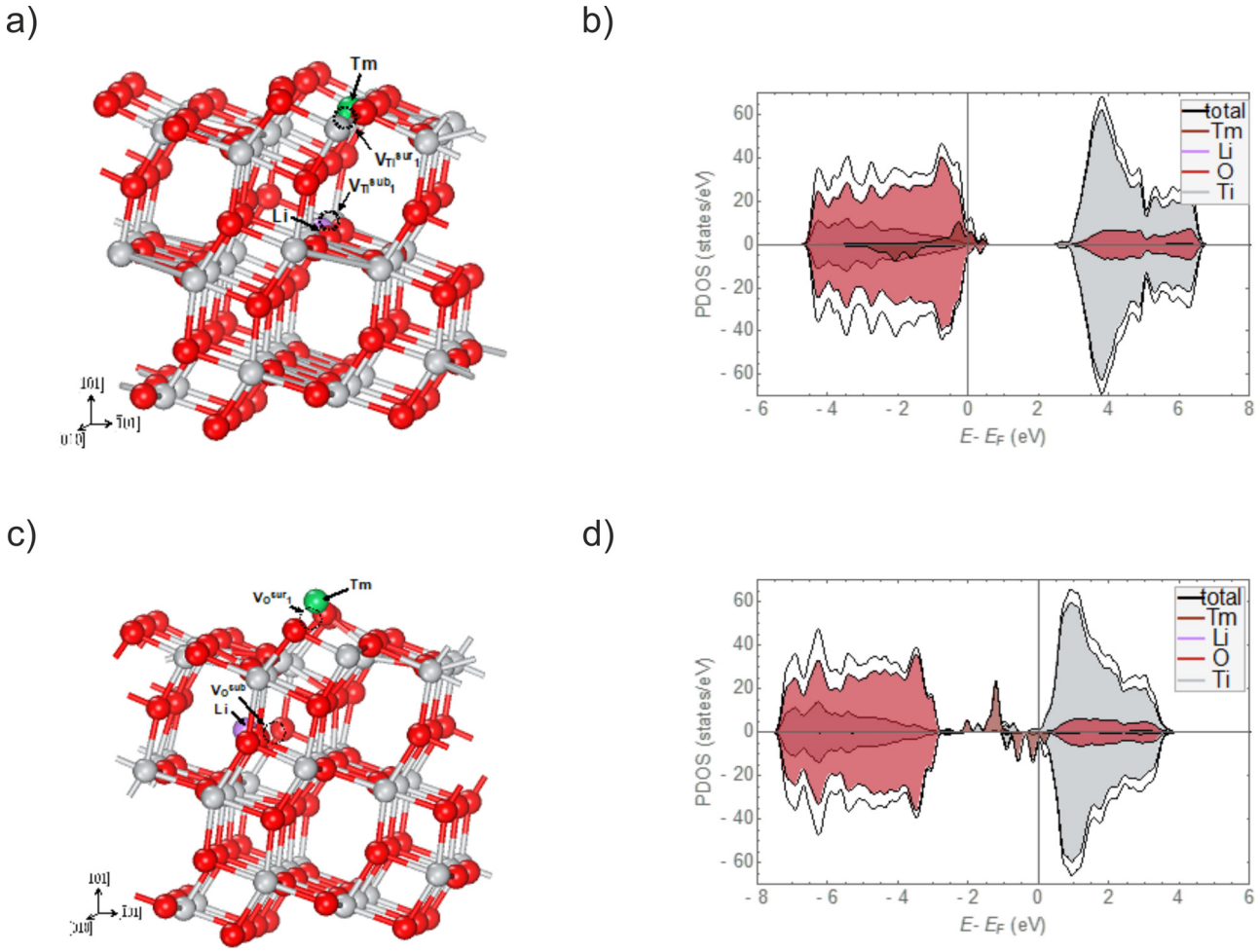

Fig. 9. Supercell slab model for (a) Tm-Li-TiO_2-V_{Ti}^{sur1}-V_{Ti}^{sub1} and (c) Tm-Li-TiO_2-V_O^{sur1}-V_O^{sub1} systems. Computed partial densities of states for (b) Tm-Li-TiO_2-V_{Ti}^{sur1}-V_{Ti}^{sub1} and (d) Tm-Li-TiO_2-V_O^{sur1} -V_O^{sub1} systems.

oxygen vacancy that acts as the centre of catalytic sites and chemisorbed species, culminating in its higher photoelectrochemical properties. In reported paper [54]. Safaei et al. proved that holes at VB of $BiVO_4$ directly oxidize water with electrons from CB of $BiVO_4$ recombining with the holes from the VB of g-C_3N_4, while the photogenerated electrons from CB of g-C_3N_4 directly reduce water.

3.7. Photocatalytic activity

The photocatalytic activity of both series of photocatalysts, namely, Tm- and Tm-Li-modified TiO_2, was investigated using a model phenol degradation reaction under irradiation with visible light ($\lambda > 420$ nm), as shown in Fig. 10 and Table 1. To obtain a full view of the photoactivity, control tests were carried out. There was no phenol degradation in the absence of either photocatalyst or visible irradiation. Thus, the results indicate that the photocatalytic activity arises from the photocatalytic activity of the prepared samples.

Fig. 10a demonstrates the photodegradation of phenol as a function of the irradiation time. The highest efficiency was achieved for the 0.25%Tm-TiO_2 sample, reaching a value of 22%. The other samples showed significantly lower photoactivities in the range from 12 to 19%. Summarizing this part of our study, the phenol degradation decreased in the following order: 0.25%Tm-TiO_2 > 0.1%Tm-TiO_2 > 0.5%Tm-TiO_2 > 1%Tm-TiO_2 > TiO_2, which indicates that the amount of thulium is of foremost importance for the obtained results. It is well known that for the modification of titania, an optimal content of modifier should be applied, with similar findings already reported, e.g., for Nd-TiO_2, Sm-TiO_2 and Er-TiO_2 [10,55,56]. This apparent drop in the photoactivity can be attributed to a higher number of recombination centres [57] and/or the blocking of the surface of the TiO_2 by an excess amount of Tm^{3+} [10].

Based on the above results, the most active sample (0.25%Tm-TiO_2) was selected for further modification with lithium ions (Li^+). Fig. 10b shows the effect of the amount of lithium on the photocatalytic

Table 4
PBE + U calculated structural parameters of doped TiO_2(101) anatase systems. Here $d_{M\text{-}O2c}$ and $d_{M\text{-}Ti5c}$ is the distance between selected atoms and corresponding surface site atoms O_{2c} and Ti_{5c}, respectively. E_{ads} is the adsorption energy of the cluster as a whole.

System name	$d_{Li\text{-}O2c}$ (Å)	$d_{Li\text{-}Ti5c}$ (Å)	$d_{Tm\text{-}O2c}$ (Å)	$d_{Tm\text{-}Ti5c}$ (Å)	E_{ads} (eV)
[a] Tm-Li-TiO_2-V_{Ti}^{sur1}-V_{Ti}^{sub1}	1.96	3.29	2.15	3.06	−5.47
[b] Tm-Li-TiO_2-V_O^{sur1}-V_O^{sub1}	2.29	3.81	2.08	3.92	−8.52

[a] Structure displayed in Fig. 8(a).
[b] Structure displayed in Fig. 8(b).

Table 5
Optimized bulk parameter, surface formation energy and Tm substitution energy for anatase TiO_2 supercell. All of the energies are in eV.

Parameter	$E^{Bulk}_{TiO_2}$	E^{Slab}_0	A (Å^2)	E^{f}_{Surf}	$E^{Slab-Tm}_{V0sur}$	$E^{Slab-Tm}_{V0sub}$	E^{sub}_{Tm}
Energy (eV)	−48.87	−1163.27	161.27	0.48 Jm^{-2}	−1160.67	−1161.05	−5.54/-5.92

properties of the 0.25%Tm-TiO_2 photocatalysts. In this case, the phenol degradation varied from 11 to 18%, and there was no significant correlation between the Li^+ content in the 0.25%Tm-TiO_2 and the photoactivity. Evidently, all samples in this series showed lower photoactivity values than the initial sample 0.25%Tm-TiO_2, although the best sample 0.25%Tm-2.0%Li-TiO_2 (18% phenol degradation) showed much better results in the up-conversion process (as described above). The reason for this rather contradictory result is still not entirely clear, but it might suggest that the up-conversion process is not responsible for the origin of the photoactivity in the visible spectrum for Tm-TiO_2, which will be discussed in more detail in the next part.

3.8. Discussion of the mechanism

3.8.1. Generation of intermediates and photostability under visible light irradiation

To follow the path of phenol degradation in the presence of all prepared photocatalysts under visible light, the formation of intermediates was determined by HPLC and studied in detail.

The amount of generated intermediates after 60 min of irradiation for all photocatalysts is presented in Fig. S1, whereas the kinetics of their formation as a function of time (for the most active sample, 0.25%Tm-TiO_2) is displayed in Fig. 11a. Evidently, the lack of intermediates in the presence of pristine TiO_2 indicates either that the loss of phenol is related to its adsorption on the titania surface or that the content of intermediates was below the detection limit of HPLC. The results of this study also indicate that catechol, hydroquinone and benzoquinone (with chemical structures shown in Fig. 11b) were primary intermediates for the phenol degradation and that for both series of samples, the highest concentration was detected for hydroquinone, which is in accordance with previous findings [58]. Both, the amount and type of intermediate products generated during degradation of phenol depends on the kinetics and type of reactive oxygen species (ROS) generated on the photocatalyst's surface [59]. Generally, resorcinol is observed when OH radicals are involved in the oxidation of phenol [60,61]. In our cause, when photocatalysts were irradiated with visible light, the main ROS involved in the process of phenol degradation over Tm- and Tm-Li-modified TiO_2 samples were $O_2^{\cdot-}$, which creates a new path to the formation of intermediate products and, consequently, phenol mineralization. Thus, along this path, the formation of resorcinol does not have to happen at all. Furthermore, for samples possessing better photoactivity, the amounts of intermediates increased, which is directly related to the rate of the photodegradation process. Fig. 11a shows the trend in the evolution of the primary intermediates in the presence of 0.25%Tm-TiO_2, where the concentrations of both catechol and benzoquinone increased with the irradiation time, whereas the hydroquinone content began to decline after 40 min of reaction.

As illustrated in Fig. 11c, the value of the phenol degradation after four successive cycles for the sample 0.25%Tm-TiO_2 was slightly lower in comparison with the result obtained after one cycle (the difference was approximately 3%). Summarizing these results and that presented in Figs. 10 and S2 it might be concluded that the obtained photocatalyst is photostable and highly efficient for oxidative decomposition of phenol under visible light.

3.8.2. Detection of reactive oxygen species generated at the photocatalyst surface

The identification and quantification of the reactive oxygen species (such as $^{\cdot}OH$ and $O_2^{\cdot-}$), generated on the surface of Tm- and Tm-Li-modified TiO_2, are essential for understanding the photocatalytic mechanisms [4]. In this regard, two types of tests were carried out, namely, $^{\cdot}OH$ generation by using terephthalic acid (TPA) for both series of prepared photocatalysts and phenol photodegradation in the presence of selected scavengers and the most active sample, with the obtained results shown in Fig. 12. In general, the fluorescence (FL) intensity registered for the Tm- and Tm-Li-modified TiO_2 samples (Fig. 12a and b) was slightly larger than that of pristine TiO_2 and negligible compared to the literature data [10,34]. Moreover, there was no correlation between the photodegradation and the amount of $^{\cdot}OH$ (a higher FL intensity means more hydroxide radicals). This apparent lack of correlation and the unnoticeable amount of $^{\cdot}OH$ can be attributed to the fact that other reactive oxygen species such as $O_2^{\cdot-}$ are also involved in the process of phenol degradation over Tm- and Tm-Li-modified TiO_2 samples. The results depicted in Fig. 12c further strengthen our conviction that the $O_2^{\cdot-}$ in the RE-TiO_2 system plays a key role. As follows, the phenol degradation in the presence of the $O_2^{\cdot-}$ scavenger decreased to near 1–2% (from 22% in the tests without scavenger), whereas the

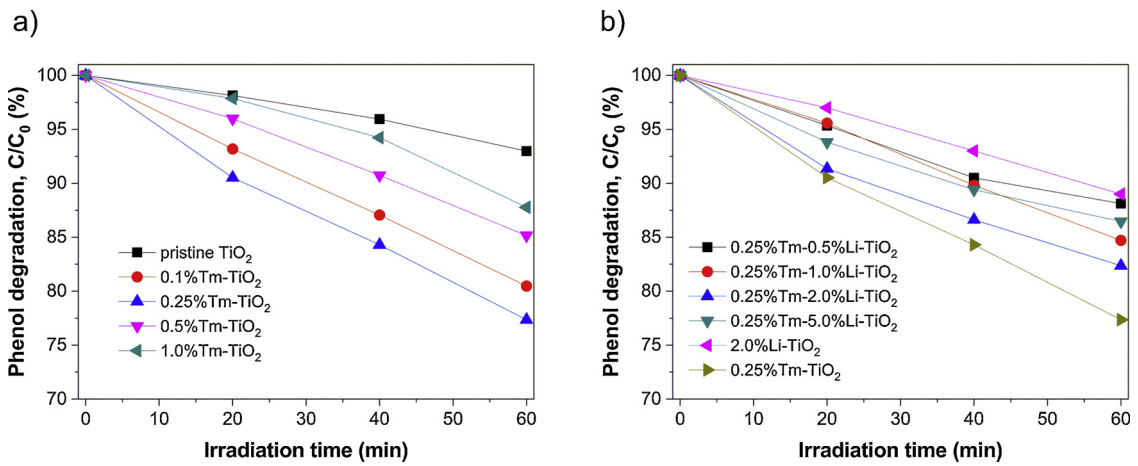

Fig. 10. Photocatalytic properties of (a) pristine TiO_2, Tm-modified TiO_2 and (b) Tm-Li-modified TiO_2 under visible light irradiation ($\lambda > 420$ nm). Test conditions: $c_0 = 0.21$ mM; m(modified-TiO_2) = 125 mg; T = 10 °C; $Q_{air} = 5$ dm^3 h^{-1}.

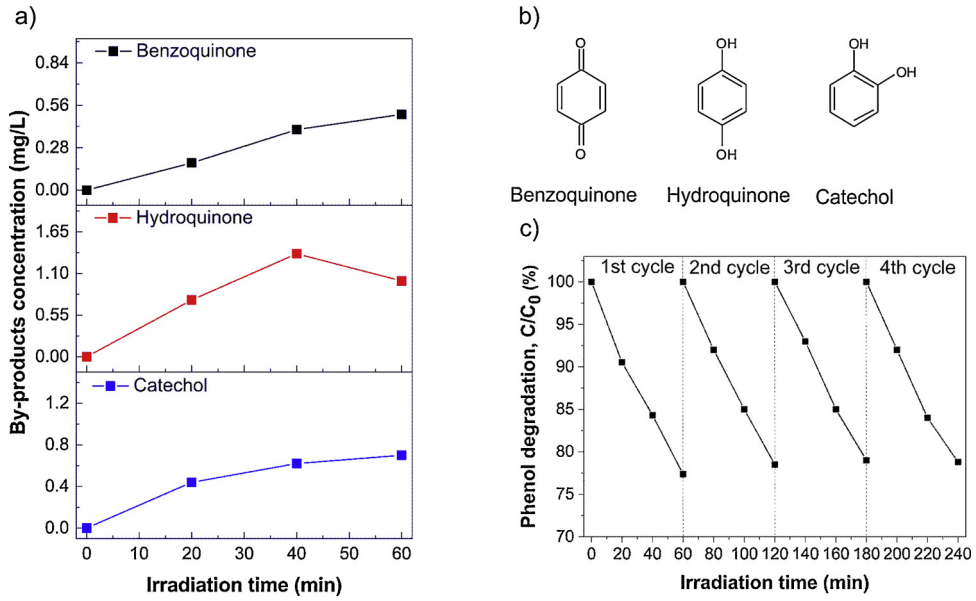

Fig. 11. (a) Evolution of primary intermediates under visible irradiation in the presence of the 0.25%-TiO_2 sample, (b) chemical structures of intermediates and (c) photostability in four cycles of the 0.25%-TiO_2 sample.

photoactivity remained almost unchanged for the h^+ and $^{\cdot}OH$ scavengers. These results are in line with previous findings [5,10].

3.8.3. Action spectra analysis

As highlighted in Fig. 13, the photoabsorption properties of Tm- and Tm-Li-modified TiO_2 remain similar to those of pristine TiO_2 (which exhibited absorption only in the UV range), maintaining a higher or lower photoactivity in polychromatic visible light ($\lambda > 420$ nm). To examine the exact visible range in which the obtained photocatalysts were excited and oxidized phenol, an action spectra analysis (AS) over 0.25%Tm-TiO_2 was performed, with the results presented in Fig. 13a–b (apparent quantum efficiency (AQE) as a function of the irradiation wavelength).

As clearly shown in Fig. 13a, the excitation of 0.25%Tm-TiO_2 in the range from 400 to 490 nm caused the photodegradation of phenol, whereas the pristine TiO_2 sample was photoactive only up to 440 nm. Irradiation with longer wavelengths up to approximately 800 nm did not contribute to the oxidation reaction. Evidently, the AQE for the 0.25%Tm-TiO_2 sample was incomparably greater than that for the pristine sample. Regarding the up-conversion process, the excitation states for Tm^{3+}, centred at 467, 685 and 795 nm (absorption peaks, see Fig. 13a), should be involved in this phenomenon. After inducing the 0.25%Tm-TiO_2 sample with the abovementioned wavelengths, a response was recorded only at 467 nm (AQE = 1.49%), with the other excited states of thulium not participating in the TiO_2 activation. This might provide adequate proof for the UCP in Tm-TiO_2. However, this sample was also photoactive in the region without absorption bands from Tm^{3+} (420, 440, 460, 480 and 490 nm). Moreover, similar results were obtained for isopropanol oxidation, as shown in Fig. 13b (same trend with phenol degradation). It should be pointed out that UCP is a multiphoton excitation and relaxation process, with the large distance between the ground and excited states of the RE ions, i.e., a possible reason for this unobservable impact of UCP on the photocatalytic activity [62,63].

According to the results obtained from luminescence spectroscopy and theoretical simulations, the Li^+ co-modification of Tm-TiO_2 enhanced the emission intensity from Tm ions, which indicates improved UCP. However, a higher photocatalytic activity for the Li-Tm-TiO_2 samples was not observed, therefore, photoactivity of these samples in visible light cannot be caused by visible-to-UV photon upconversion (as shown in Fig. 13c) and excitation of pristine TiO_2. Fig. 7 provides additional support for mentioned hypothesis, there was no emission in the UV region after excitation of Tm-TiO_2 or Li-Tm-TiO_2 by wavelengths from the visible range. On the other hand, photoactivity of 0.25%Tm-TiO_2 was higher in comparison with 0.25%Tm-2.0%Li-TiO_2, which is likely due to an excessive enrichment of Tm-TiO_2 surface with either very fine Li nanoclusters or atomically dispersed lithium (discussed in detail in XPS part) and blocking the surface against visible irradiation since the PL intensity (Fig. 6) was comparable (higher intensity of Li-Tm-TiO_2 than Tm-TiO_2 system could suggest higher charge carrier recombination and cause lower photoactivity). Based on the results obtained from UV–vis, BET specific surface measurements, XRD and XPS,

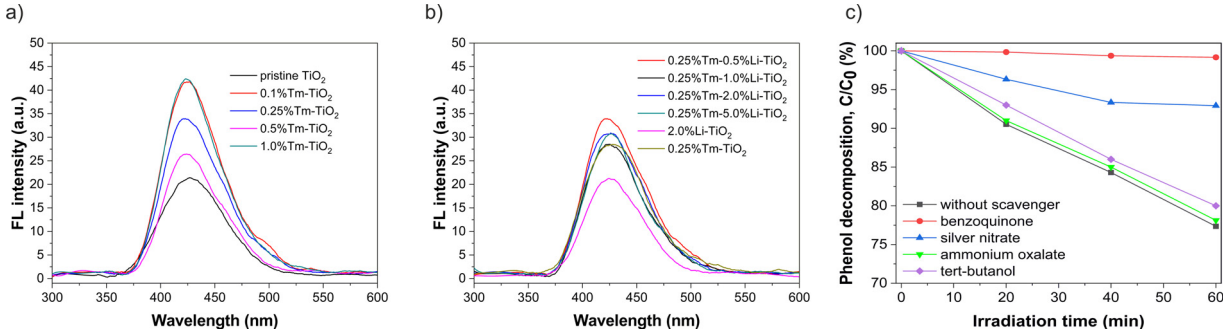

Fig. 12. Efficiency of $^{\cdot}OH$ generation using TPA for (a) Tm-TiO_2, (b) Tm-Li-TiO_2 and (c) phenol degradation containing scavengers under visible light irradiation.

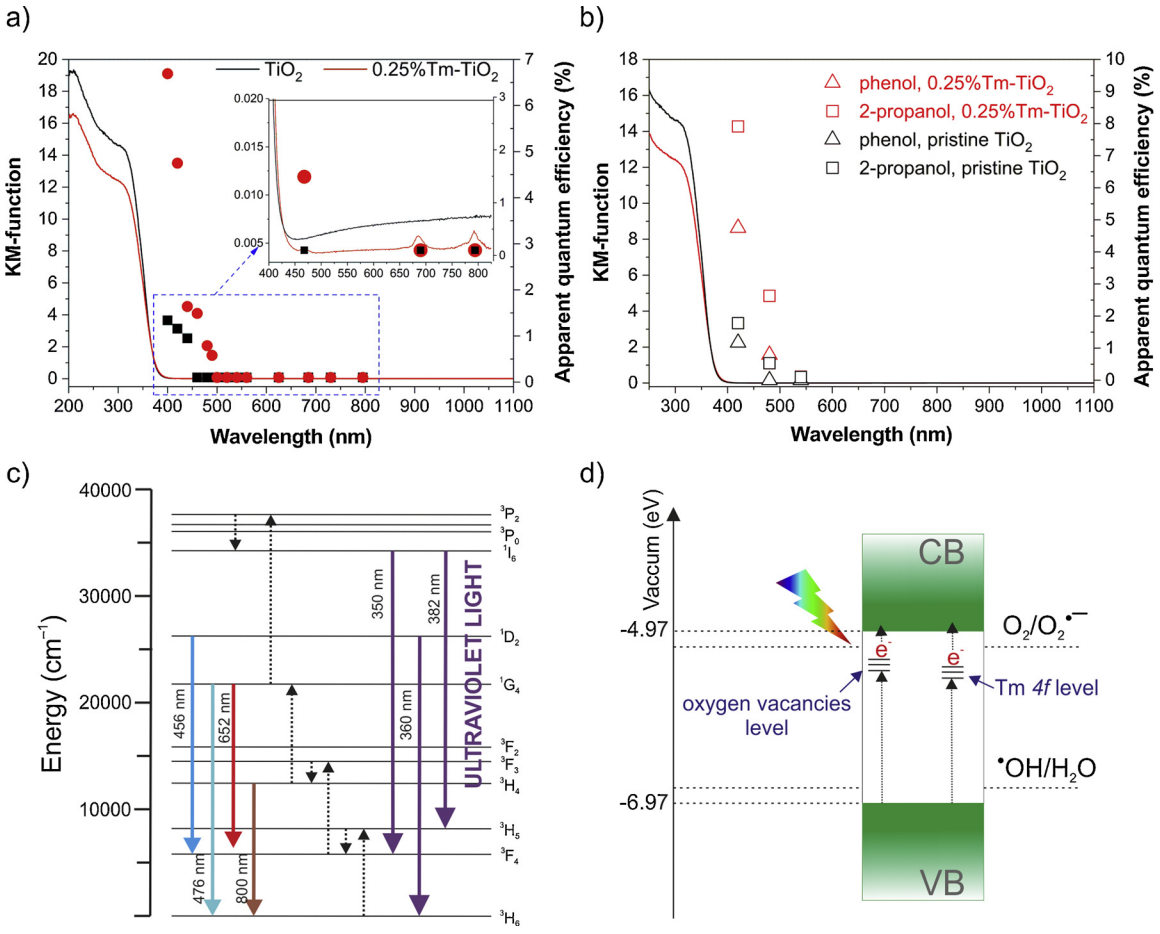

Fig. 13. Action spectra analysis of the process of phenol oxidation over 0.25%Tm-TiO_2 sample: (a) detailed mechanism, (b) action spectra for phenol and isopropanol oxidation, (c) simplified energy level diagrams of excitation path for the up-conversion emission of ultraviolet light under 980 nm excitation according to [5], and (d) proposed excitation mechanism of Tm-TiO_2 under visible light. Apparent quantum efficiency: squares, triangles and circles; photoabsorption presented as K–M function: lines.

it is possible to draw the conclusion that the Tm-modification of TiO_2 causes an increase in the BET surface area and that the redshift of the absorption band of TiO_2 occurs according to a charge-transfer transition between the Tm *f* electrons and the titanium dioxide conduction/valence band or/and due to the creation of extrinsic defects in the grain boundaries. In addition, the synergistic effects of new Tm-*f* states and surface vacancies may further reduce the photon excitation energy from the VB to the CB. Our results seem to confirm abovementioned hypotheses since: *(1)* computed partial densities of states confirmed a new sub-band gap states from the Tm *4f* level (see Figs. 8 and 9) and *(2)* amount of Ti^{3+} form XPS analysis was much higher (more than twice) in Tm-TiO_2 or Li-Tm-TiO_2 (3.9 or 4.6%, respectively) than in pristine TiO_2 (1.9%). The presence of large amount of Ti^{3+} may cause the emergence of a new state associated with oxygen vacancies located below CB of TiO_2, according to [64] and our results (see Figs. 8 and 9) and reduce the irradiation wavelength needed to excite the photocatalyst. To summarize presented work, the proposed photocatalytic mechanism of the Tm-TiO_2 excitation under visible light is presented in Fig. 13d. The VB and CB edge positions of Li-Tm-TiO_2 system ca. at 1.01 and 3.02 eV (vs vacuum), respectively. It is proposed that the electrons can be excited from the TiO_2 valence band to the formed sub-band gap states from the lanthanide *4f* level (that lies below the conduction band of the semiconductor) or oxygen vacancies under visible light irradiation. Then trapped electrons can react with O_2 and form reactive oxygen species, such as $O_2^{\bullet -}$, leading to organic pollutant degradation. Therefore, visible light becomes energetic enough to facilitate the abovementioned electron transitions due to the lower energy demand between the new energy levels and the valence band.

4. Conclusions

Nanostructured TiO_2 co-modified with Tm and Li was obtained by the hydrothermal method. According to luminescence spectroscopy and theoretical simulations, the Li^+ co-modification of Tm-TiO_2 enhanced the emission intensity from Tm ions. The Tm ions were located at the crystal boundaries rather than inside the TiO_2 unit cell, where Tm surface doping was observed. The Tm-TiO_2 samples showed a higher BET surface area, a redshift of the absorption edge, and a higher concentration of surface defects in comparison to pristine TiO_2. The highest photocatalytic activity for phenol degradation under Vis irradiation was observed for a 0.25% Tm-TiO_2 sample, with stable photocatalytic activity over four cycles. It is proposed that the formation of sub-band gap states from the lanthanide *4f* level plays a key role in the organic pollutant degradation process under Vis light irradiation. The Li^+ co-modification of Tm-TiO_2 reduced the photocatalytic activity of the Tm-TiO_2 system under Vis irradiation, probably due to the higher charge carrier recombination on the TiO_2 surface. Although, the action spectra revealed that the excitation of Tm-TiO_2 in the range from 400 to 490 nm caused the photodegradation of the phenol, the influence of the UCP on photocatalytic activity was not observed.

Acknowledgements

This research was financially supported by the Polish National

Science Centre (grant No. NCN 2015/17/D/ST5/01331) and supported by the Foundation for Polish Science (FNP). The authors gratefully acknowledge support and computational resources from the Interdisciplinary Center for Nanotoxicity at Jackson State University and KDM CI TASK. A.M. thanks the *National Science Center* (no. 2015/19/N/NZ7/01593) for financial support. The authors thank Professor Bunsho Ohtani for sound advice, fruitful discussion and unlimited access to laboratory equipment, and Dr. Maya Endo-Kimura for STEM analysis. The authors thank Professor Jerzy Leszczynski for his support in theoretical simulations and enabling research in collaboration with members of ICN's team.

Appendix A. Supplementary data

Supplementary material related to this article can be found, in the online version, at doi:https://doi.org/10.1016/j.apcatb.2019.03.051.

References

[1] J. Schneider, M. Matsuoka, M. Takeuchi, J. Zhang, Y. Horiuchi, M. Anpo, D.W. Bahnemann, Understanding TiO2 photocatalysis: mechanisms and materials, Chem. Rev. 114 (2014) 9919–9986, https://doi.org/10.1021/cr5001892.

[2] A. Mishra, A. Mehta, S. Basu, Clay supported TiO2 nanoparticles for photocatalytic degradation of environmental pollutants: a review, J. Environ. Chem. Eng. 6 (2018) 6088–6107, https://doi.org/10.1016/j.jece.2018.09.029.

[3] Z. Xing, J. Zhang, J. Cui, J. Yin, T. Zhao, J. Kuang, Z. Xiu, N. Wan, W. Zhou, Recent advances in floating TiO2-based photocatalysts for environmental application, Appl. Catal. B Environ. 225 (2018) 452–467, https://doi.org/10.1016/j.apcatb.2017.12.005.

[4] J. Reszczyńska, T. Grzyb, J.W. Sobczak, W. Lisowski, M. Gazda, B. Ohtani, A. Zaleska, Visible light activity of rare earth metal doped (Er3+, Yb3+ or Er3+/Yb3+) titania photocatalysts, Appl. Catal. B Environ. 163 (2015) 40–49, https://doi.org/10.1016/j.apcatb.2014.07.010.

[5] P. Mazierski, A. Mikolajczyk, B. Bajorowicz, A. Malankowska, A. Zaleska-Medynska, J. Nadolna, The role of lanthanides in TiO2-based photocatalysis: a review, Appl. Catal. B Environ. 233 (2018) 301–317, https://doi.org/10.1016/j.apcatb.2018.04.019.

[6] J. Reszczyńska, T. Grzyb, J.W. Sobczak, W. Lisowski, M. Gazda, B. Ohtani, A. Zaleska, Lanthanide co-doped TiO2: the effect of metal type and amount on surface properties and photocatalytic activity, Appl. Surf. Sci. 307 (2014) 333–345, https://doi.org/10.1016/j.apsusc.2014.03.199.

[7] J. Navas, A. Sánchez-Coronilla, T. Aguilar, D.M. De los Santos, N.C. Hernández, R. Alcántara, C. Fernández-Lorenzo, J. Martín-Calleja, Thermo-selective Tm $_x$ Ti $_{1-x}$ O $_{2-x/2}$ nanoparticles: from Tm-doped anatase TiO $_2$ to a rutile/pyrochlore Tm $_2$ Ti $_2$ O $_7$ mixture. An experimental and theoretical study with a photoca, Nanoscale 6 (2014) 12740–12757, https://doi.org/10.1039/C4NR03715D.

[8] D.M. de los Santos, J. Navas, T. Aguilar, A. Sánchez-Coronilla, R. Alcántara, C. Fernández-Lorenzo, G. Blanco, J.M. Calleja, Study of thulium doping effect and enhancement of photocatalytic activity of rutile TiO2 nanoparticles, Mater. Chem. Phys. 161 (2015) 175–184, https://doi.org/10.1016/j.matchemphys.2015.05.034.

[9] D.M. de los Santos, J. Navas, T. Aguilar, A. Sánchez-Coronilla, C. Fernández-Lorenzo, R. Alcántara, J.C. Piñero, G. Blanco, J. Martín-Calleja, Tm-doped TiO2 and Tm2Ti2O7 pyrochlore nanoparticles: enhancing the photocatalytic activity of rutile with a pyrochlore phase, Beilstein J. Nanotechnol. 6 (2015) 605–616, https://doi.org/10.3762/bjnano.6.62.

[10] J.N. Patrycja Parnicka, Paweł Mazierski, Tomasz Grzyb, Zhishun Wei, Ewa Kowalska, Bushio Ohtani, Tomasz Klimczuk, Adriana Zaleska-Medynska, Preparation and photocatalytic activity of Nd-modified TiO2 photocatalysts: insight into the excitation mechanism under visible light, J. Catal. (2017).

[11] F. Pavón, A. Urbieta, P. Fernández, Luminescence and light guiding properties of Er and Li codoped ZnO nanostructures, J. Lumin. 195 (2018) 396–401, https://doi.org/10.1016/j.jlumin.2017.11.059.

[12] S. Bachir, K. Azuma, J. Kossanyi, P. Valat, J.C. Ronfard-Haret, Photoluminescence of polycrystalline zinc oxide co-activated with trivalent rare earth ions and lithium. Insertion of rare-earth ions into zinc oxide, J. Lumin. 75 (1997) 35–49, https://doi.org/10.1016/S0022-2313(97)00093-8.

[13] T.V. Gavrilović, D.J. Jovanović, L.V. Trandafilović, M.D. Dramićanin, Effects of Ho3+ and Yb3+ doping concentrations and Li+ co-doping on the luminescence of GdVO4 powders, Opt. Mater. (Amst.) 45 (2015) 76–81, https://doi.org/10.1016/j.optmat.2015.03.013.

[14] B. Milićević, V. Đorđević, K. Vuković, G. Dražić, M.D. Dramićanin, Effects of Li+ co-doping on properties of Eu3+ activated TiO2 anatase nanoparticles, Opt. Mater. (Amst). 72 (2017) 316–322, https://doi.org/10.1016/j.optmat.2017.06.029.

[15] G. Kresse, J. Furthmüller, Efficiency of ab-initio total energy calculations for metals and semiconductors using a plane-wave basis set, Comput. Mater. Sci. 6 (1996) 15–50, https://doi.org/10.1016/0927-0256(96)00008-0.

[16] J.P. Perdew, J.A. Chevary, S.H. Vosko, K.A. Jackson, M.R. Pederson, D.J. Singh, C. Fiolhais, Atoms, molecules, solids, and surfaces: applications of the generalized gradient approximation for exchange and correlation, Phys. Rev. B 46 (1992) 6671–6687, https://doi.org/10.1103/PhysRevB.46.6671.

[17] A. Krukowska, M.J. Winiarski, J. Strychalska-Nowak, T. Klimczuk, W. Lisowski, A. Mikolajczyk, H.P. Pinto, T. Puzyn, T. Grzyb, A. Zaleska-Medynska, Rare earth ions doped K2Ta2O6 photocatalysts with enhanced UV–vis light activity, Appl. Catal. B Environ. 224 (2018) 451–468, https://doi.org/10.1016/j.apcatb.2017.10.061.

[18] A. Mikolajczyk, H.P. Pinto, A. Gajewicz, J. Leszczynski, *Ab initio* studies of anatase TiO_2 (101) surface-supported Au_8 clusters, Curr. Top. Med. Chem. 15 (2015) 1859–1867, https://doi.org/10.2174/1568026615666150506151826.

[19] F.F. Sanches, G. Mallia, L. Liborio, U. Diebold, N.M. Harrison, Hybrid exchange density functional study of vicinal anatase $\mathrm{Ti}{\mathrm{O}}_{2}$ surfaces, Phys. Rev. B 89 (2014) 245309, , https://doi.org/10.1103/PhysRevB.89.245309.

[20] P. Mazierski, J. Nadolna, G. Nowaczyk, W. Lisowski, M.J. Winiarski, T. Klimczuk, M.P. Kobylański, S. Jurga, A. Zaleska-Medynska, Highly visible-light-Photoactive heterojunction based on TiO2 nanotubes decorated by Pt nanoparticles and Bi2S3 quantum dots, J. Phys. Chem. C 121 (2017) 17215–17225, https://doi.org/10.1021/acs.jpcc.7b03895.

[21] P. Mazierski, J. Nadolna, W. Lisowski, M.J. Winiarski, M. Gazda, M. Nischk, T. Klimczuk, A. Zaleska-Medynska, Effect of irradiation intensity and initial pollutant concentration on gas phase photocatalytic activity of TiO2 nanotube arrays, Catal. Today 284 (2017) 19–26, https://doi.org/10.1016/j.cattod.2016.09.004.

[22] P. Parnicka, P. Mazierski, T. Grzyb, W. Lisowski, E. Kowalska, B. Ohtani, A. Zaleska-Medynska, J. Nadolna, Influence of the preparation method on the photocatalytic activity of Nd-modified TiO2, Beilstein J. Nanotechnol. 9 (2018) 447–459, https://doi.org/10.3762/bjnano.9.43.

[23] a Xu, The Preparation, Characterization, and their photocatalytic activities of rare-earth-Doped TiO2 nanoparticles, J. Catal. 207 (2002) 151–157, https://doi.org/10.1006/jcat.2002.3539.

[24] J. Sivasankari, S. Sankar, S. Selvakumar, L. Vimaladevi, R. Krithiga, Synthesis, structural and optical properties of Er doped, Li doped and Er + Li co-doped ZnO nanocrystallites by solution-combustion method, Mater. Chem. Phys. 143 (2014) 1528–1535, https://doi.org/10.1016/j.matchemphys.2013.12.015.

[25] P. Peterka, I. Kasik, A. Dhar, B. Dussardier, W. Blanc, Theoretical Modeling of Fiber Laser at 810 Nm Based on Thulium-Doped Silica Fibers with Enhanced 3H4 Level Lifetime, (2011), https://doi.org/10.1364/OE.19.002773.

[26] M. Grujić-Brojčin, S. Armaković, N. Tomić, B. Abramović, A. Golubović, B. Stojadinović, A. Kremenović, B. Babić, Z. Dohčević-Mitrović, M. Šćepanović, Surface modification of sol–gel synthesized TiO2 nanoparticles induced by La-doping, Mater. Charact. 88 (2014) 30–41, https://doi.org/10.1016/j.matchar.2013.12.002.

[27] J. Reszczyńska, T. Grzyb, Z. Wei, M. Klein, E. Kowalska, B. Ohtani, A. Zaleska-Medynska, Photocatalytic activity and luminescence properties of RE3+–TiO2 nanocrystals prepared by sol–gel and hydrothermal methods, Appl. Catal. B Environ. 181 (2016) 825–837, https://doi.org/10.1016/j.apcatb.2015.09.001.

[28] S.J. Armaković, M. Grujić-Brojčin, M. Šćepanović, S. Armaković, A. Golubović, B. Babić, B.F. Abramović, Efficiency of La-doped TiO2 calcined at different temperatures in photocatalytic degradation of β-blockers, Arab. J. Chem. (2017), https://doi.org/10.1016/j.arabjc.2017.01.001.

[29] B. Trujillo-Navarrete, M. del Pilar Haro-Vázquez, R.M. Félix-Navarro, F. Paraguay-Delgado, H. Alvarez-Huerta, S. Pérez-Sicairos, E.A. Reynoso-Soto, Effect of Nd3+ doping on structure, microstructure, lattice distortion and electronic properties of TiO2 nanoparticles, J. Rare Earths. 35 (2017) 259–270, https://doi.org/10.1016/S1002-0721(17)60909-8.

[30] J. Reszczynska, D. Arenas Esteban, M. Gazda, A. Zaleska, Pr-doped TiO < inf > 2 < /inf > . The effect of metal content on photocatalytic activity, Physicochem. Probl. Miner. Process. 50 (2014), https://doi.org/10.5277/ppmp140208.

[31] G.L. Kabongo, G.H. Mhlongo, B.M. Mothudi, K.T. Hillie, P.S. Mbule, M.S. Dhlamini, Structural, photoluminescence and XPS properties of Tm3+ ions in ZnO nanostructures, J. Lumin. 187 (2017) 141–153, https://doi.org/10.1016/j.jlumin.2017.02.024.

[32] Z. Wei, M. Endo, K. Wang, E. Charbit, A. Markowska-Szczupak, B. Ohtani, E. Kowalska, Noble metal-modified octahedral anatase titania particles with enhanced activity for decomposition of chemical and microbiological pollutants, Chem. Eng. J. 318 (2017) 121–134, https://doi.org/10.1016/j.cej.2016.05.138.

[33] J. Yu, X. Zhao, Q. Zhao, Effect of surface structure on photocatalytic activity of TiO2 thin films prepared by sol-gel method, Thin Solid Films 379 (2000) 7–14, https://doi.org/10.1016/S0040-6090(00)01542-X.

[34] P. Mazierski, M. Nischk, M. Gołkowska, W. Lisowski, M. Gazda, M.J.M.J. Winiarski, T. Klimczuk, A. Zaleska-Medynska, Photocatalytic activity of nitrogen doped TiO2 nanotubes prepared by anodic oxidation: the effect of applied voltage, anodization time and amount of nitrogen dopant, Appl. Catal. B Environ. 196 (2016) 77–88, https://doi.org/10.1016/j.apcatb.2016.05.006.

[35] P. Gorska, a Zaleska, a Suska, J. Hupka, Photocatalytic activity and surface properties of carbon-doped titanium dioxide, Physicochem. Probl. Miner. Process. 43 (2009) 21–30.

[36] D. Li, H. Haneda, S. Hishita, N. Ohashi, Visible-light-driven N−F−Codoped TiO2 photocatalysts. 2. Optical characterization, photocatalysis, and potential application to air purification, Chem. Mater. 17 (2005) 2596–2602, https://doi.org/10.1021/cm049099p.

[37] S. Obregón, A. Kubacka, M. Fernández-García, G. Colón, High-performance Er3+-TiO2system: dual up-conversion and electronic role of the lanthanide, J. Catal. 299 (2013) 298–306, https://doi.org/10.1016/j.jcat.2012.12.021.

[38] C.M. Trindade, F.G. Rego-Filho, N.G.C. Astrath, C. Jacinto, A.S. Gouveia-Neto, UV–visible-NIR light generation through frequency upconversion in Tm3+-doped low silica calcium aluminosilicate glasses using multiple excitation around 1.2 μm,

J. Solid State Chem. 260 (2018) 147–150, https://doi.org/10.1016/j.jssc.2018.01.012.
[39] L. BIAN, M. SONG, T. ZHOU, X. ZHAO, Q. DAI, Band gap calculation and photo catalytic activity of rare earths doped rutile TiO2, J. Rare Earths. 27 (2009) 461–468, https://doi.org/10.1016/S1002-0721(08)60270-7.
[40] P. Mazierski, W. Lisowski, T. Grzyb, M.J. Winiarski, T. Klimczuk, A. Mikołajczyk, J. Flisikowski, A. Hirsch, A. Kołakowska, T. Puzyn, A. Zaleska-Medynska, J. Nadolna, Enhanced photocatalytic properties of lanthanide-TiO2 nanotubes: an experimental and theoretical study, Appl. Catal. B Environ. 205 (2017) 376–385, https://doi.org/10.1016/j.apcatb.2016.12.044.
[41] F.J. Knorr, J.L. McHale, Spectroelectrochemical photoluminescence of trap states of nanocrystalline TiO2 in aqueous media, J. Phys. Chem. C. 117 (2013) 13654–13662, https://doi.org/10.1021/jp402264p.
[42] B. Zhou, H. Lin, E.Y.-B. Pun, Tm3 + -doped tellurite glasses for fiber amplifiers in broadband optical communication at 1.20 μm wavelength region, Opt. Express 18 (2010) 18805–18810, https://doi.org/10.1364/OE.18.018805.
[43] C. Görller-Walrand, K. Binnemans, Spectral intensities of f-f transitions, Handb. Phys. Chem. Rare Earths, (1998), pp. 101–264, https://doi.org/10.1016/S0168-1273(98)25006-9.
[44] M. Misiak, K. Prorok, B. Cichy, A. Bednarkiewicz, W. Stręk, Thulium concentration quenching in the up-converting α-Tm3 + /Yb3 + NaYF4 colloidal nanocrystals, Opt. Mater. (Amst.) 35 (2013) 1124–1128, https://doi.org/10.1016/j.optmat.2013.01.002.
[45] D.K. Xu, C.F. Liu, J.W. Yan, H.Q. Ouyang, S.H. Yang, Y.L. Zhang, Enhanced near-infrared upconversion emission of Yb3 + -Tm3 + Co-doped Gd2O3 sub-microrods, Phys. Procedia 76 (2015) 160–164, https://doi.org/10.1016/j.phpro.2015.10.029.
[46] Q. Cheng, J. Sui, W. Cai, Enhanced upconversion emission in Yb3 + and Er3 + codoped NaGdF4 nanocrystals by introducing Li + ions, Nanoscale 4 (2012) 779, https://doi.org/10.1039/c1nr11365h.
[47] a.N. Meza-Rocha, E.F. Huerta, U. Caldiño, S. Carmona-Téllez, M. Bettinelli, A. Speghini, S. Pelli, G.C. Righini, C. Falcony, Dependence of the up-conversion emission of Li + co-doped Y2O3:Er3 + films with dopant concentration, J. Lumin. 167 (2015) 352–359, https://doi.org/10.1016/j.jlumin.2015.07.003.
[48] J.P. Perdew, Density functional theory and the band gap problem, Int. J. Quantum Chem. 28 (1985) 497–523, https://doi.org/10.1002/qua.560280846.
[49] D. Bagayoko, Understanding density functional theory (DFT) and completing it in practice, AIP Adv. 4 (2014) 127104, , https://doi.org/10.1063/1.4903408.
[50] H. Ullah, A.A. Tahir, T.K. Mallick, Polypyrrole/TiO2 composites for the application of photocatalysis, Sens. Actuators B Chem. 241 (2017) 1161–1169, https://doi.org/10.1016/j.snb.2016.10.019.
[51] H. Ullah, Inter-molecular interaction in Polypyrrole/TiO2: a DFT study, J. Alloys Compd. 692 (2017) 140–148, https://doi.org/10.1016/j.jallcom.2016.08.169.
[52] H. Ullah, A.A. Tahir, T.K. Mallick, Structural and electronic properties of oxygen defective and Se-doped p-type BiVO4(001) thin film for the applications of photocatalysis, Appl. Catal. B Environ. 224 (2018) 895–903, https://doi.org/10.1016/j.apcatb.2017.11.034.
[53] S.N.F.M. Nasir, H. Ullah, M. Ebadi, A.A. Tahir, J.S. Sagu, M.A. Mat Teridi, new insights into Se/BiVO4 heterostructure for photoelectrochemical water splitting: a combined experimental and DFT study, J. Phys. Chem. C 121 (2017) 6218–6228, https://doi.org/10.1021/acs.jpcc.7b01149.
[54] J. Safaei, H. Ullah, N.A. Mohamed, M.F.M. Noh, M.F. Soh, A.A. Tahir, N.A. Ludin, M.A. Ibrahim, W.N.R.W. Isahak, M.A.M. Teridi, Enhanced photoelectrochemical performance of Z-scheme g-C3N4/BiVO4 photocatalyst, Appl. Catal. B Environ. 234 (2018) 296–310, https://doi.org/10.1016/j.apcatb.2018.04.056.
[55] Q. Xiao, Z. Si, Z. Yu, G. Qiu, Sol–gel auto-combustion synthesis of samarium-doped TiO2 nanoparticles and their photocatalytic activity under visible light irradiation, Mater. Sci. Eng. B 137 (2007) 189–194, https://doi.org/10.1016/j.mseb.2006.11.011.
[56] J. Reszczynska, A. Iwulska, G. Sliwinski, A. Zaleska, Characterization and photocatalytic activity of rare earth metal-doped titanium dioxide, Physicochem. Problems Miner. Process. 48 (2012) 201–208.
[57] Y. Yang, C. Zhang, Y. Xu, H. Wang, X. Li, C. Wang, Electrospun Er:TiO2 nanofibrous films as efficient photocatalysts under solar simulated light, Mater. Lett. 64 (2010) 147–150, https://doi.org/10.1016/j.matlet.2009.10.028.
[58] O. Tahiri Alaoui, A. Herissan, C. Le Quoc, Mel M. Zekri, S. Sorgues, H. Remita, C. Colbeau-Justin, Elaboration, charge-carrier lifetimes and activity of Pd-TiO2 photocatalysts obtained by gamma radiolysis, J. Photochem. Photobiol. A: Chem. 242 (2012) 34–43, https://doi.org/10.1016/j.jphotochem.2012.05.030.
[59] P. Mazierski, A. Malankowska, M. Kobylański, M. Diak, M. Kozak, M.J. Winiarski, T. Klimczuk, W. Lisowski, G. Nowaczyk, A. Zaleska-Medynska, Photocatalytically active TiO2/Ag2O nanotube arrays interlaced with silver nanoparticles obtained from the one-step anodic oxidation of Ti?Ag alloys, ACS Catal. (2017) 2753–2764, https://doi.org/10.1021/acscatal.7b00056.
[60] A. Sobczyński, L. Duczmal, W. Zmudziński, Phenol destruction by photocatalysis on TiO2: an attempt to solve the reaction mechanism, J. Mol. Catal. A Chem. 213 (2004) 225–230, https://doi.org/10.1016/j.molcata.2003.12.006.
[61] S. Ahmed, M.G. Rasul, W.N. Martens, R. Brown, M.A. Hashib, Heterogeneous photocatalytic degradation of phenols in wastewater: a review on current status and developments, Desalination 261 (2010) 3–18, https://doi.org/10.1016/j.desal.2010.04.062.
[62] R. Balda, J. Fernández, E.E. Nyein, U. Hömmerich, Infrared to visible upconversion of Nd 3 + ions in KPb 2 Br 5 low phonon crystal, Opt. Express 14 (2006) 3993–4004, https://doi.org/10.1364/OE.14.003993.
[63] P.V. Ramakrishna, S.V.N. Pammi, K. Samatha, UV–visible upconversion studies of Nd3 + ions in lead tellurite glass, Solid State Commun. 155 (2013) 21–24, https://doi.org/10.1016/j.ssc.2012.10.043.
[64] X. Chen, L. Liu, F. Huang, Black titanium dioxide (TiO2) nanomaterials, Chem. Soc. Rev. 44 (2015) 1861–1885, https://doi.org/10.1039/C4CS00330F.